

RESEARCH

Open Access



Epigenetic reactivation of tumor suppressor genes with CRISPRa technologies as precision therapy for hepatocellular carcinoma

Agustin Sgro^{1,2,3} , Joseph Cursons⁴ , Charlene Waryah^{1,2} , Eleanor A. Woodward^{1,2} ,
Momenh Foroutan⁴ , Ruqian Lyu^{5,6} , George C. T. Yeoh^{2,7} , Peter J. Leedman^{2,8,9}  and
Pilar Blancafort^{1,2,3*} 

Abstract

Background Epigenetic silencing of tumor suppressor genes (TSGs) is a key feature of oncogenesis in hepatocellular carcinoma (HCC). Liver-targeted delivery of CRISPR-activation (CRISPRa) systems makes it possible to exploit chromatin plasticity, by reprogramming transcriptional dysregulation.

Results Using The Cancer Genome Atlas HCC data, we identify 12 putative TSGs with negative associations between promoter DNA methylation and transcript abundance, with limited genetic alterations. All HCC samples harbor at least one silenced TSG, suggesting that combining a specific panel of genomic targets could maximize efficacy, and potentially improve outcomes as a personalized treatment strategy for HCC patients. Unlike epigenetic modifying drugs lacking locus selectivity, CRISPRa systems enable potent and precise reactivation of at least 4 TSGs tailored to representative HCC lines. Concerted reactivation of *HHIP*, *MT1M*, *PZP*, and *TTC36* in Hep3B cells inhibits multiple facets of HCC pathogenesis, such as cell viability, proliferation, and migration.

Conclusions By combining multiple effector domains, we demonstrate the utility of a CRISPRa toolbox of epigenetic effectors and gRNAs for patient-specific treatment of aggressive HCC.

Keywords CRISPRa, Genome multiplexing, Epigenetic editing toolbox, Tumor suppressor genes, Hepatocellular carcinoma, Epigenetic drugs, Precision medicine

*Correspondence:

Pilar Blancafort
pilar.blancafort@uwa.edu.au

¹ Cancer Epigenetics Group, The Harry Perkins Institute of Medical Research, Nedlands, Perth, WA 6009, Australia

² Centre for Medical Research, The University of Western Australia, Perth, WA 6009, Australia

³ School of Human Sciences, The University of Western Australia, Crawley, Perth, WA 6009, Australia

⁴ Biomedicine Discovery Institute and the Department of Biochemistry and Molecular Biology, Monash University, Clayton, VIC 3800, Australia

⁵ Bioinformatics and Cellular Genomics, St Vincent's Institute of Medical Research, Fitzroy, Melbourne, VIC 3065, Australia

⁶ Melbourne Integrative Genomics/School of Mathematics and Statistics, Faculty of Science, The University of Melbourne, Royal Parade, Parkville, VIC 3010, Australia

⁷ School of Molecular Sciences, University of Western Australia, Crawley, Perth, WA 6009, Australia

⁸ Laboratory for Cancer Medicine, Harry Perkins Institute of Medical Research, QEII Medical Centre, 6 Verdun St, Nedlands, Perth, WA 6009, Australia

⁹ School of Medicine and Pharmacology, The University of Western Australia, Crawley, Perth, WA 6009, Australia



© The Author(s) 2023. **Open Access** This article is licensed under a Creative Commons Attribution 4.0 International License, which permits use, sharing, adaptation, distribution and reproduction in any medium or format, as long as you give appropriate credit to the original author(s) and the source, provide a link to the Creative Commons licence, and indicate if changes were made. The images or other third party material in this article are included in the article's Creative Commons licence, unless indicated otherwise in a credit line to the material. If material is not included in the article's Creative Commons licence and your intended use is not permitted by statutory regulation or exceeds the permitted use, you will need to obtain permission directly from the copyright holder. To view a copy of this licence, visit <http://creativecommons.org/licenses/by/4.0/>. The Creative Commons Public Domain Dedication waiver (<http://creativecommons.org/publicdomain/zero/1.0/>) applies to the data made available in this article, unless otherwise stated in a credit line to the data.

Background

Hepatocellular carcinoma (HCC) is the most prevalent form of liver cancer and the third most lethal cancer worldwide [1]. Chronic liver inflammation progressively induces fibrosis leading to cirrhosis and ultimately, in a small percentage of people, HCC [2]. During this process, hepatocytes acquire multiple genetic and epigenetic alterations [3, 4]. Furthermore, a diverse range of etiologies such as viral hepatitis B and C infections, the metabolic syndrome, diabetes, obesity, non-alcoholic steatohepatitis, and chronic alcohol consumption contribute to the pathogenesis and development of HCC [5].

Early stages of HCC are treated with potentially curative locoregional therapies; however, high rates of recurrence (70%) 5 years post-hepatic resection constitute a serious impasse, and adjuvant treatments to prevent relapse represent a still unmet medical need [6]. There are six approved systemic therapies for the management of advanced unresectable HCC. First-line treatments include the multi-kinase inhibitors, such as sorafenib and lenvatinib, and the combination of atezolizumab (anti-PD-L1) and bevacizumab (anti-VEGF-A) antibodies. For non-responders, the second-line single-agent regimens consist of multi-kinase inhibitors, such as regorafenib, cabozantinib, or ramucirumab (anti-VEGFR2 antibody). Emerging FDA-approved immune therapies include checkpoint blockades, such as nivolumab and pembrolizumab (anti-PD-1), and the combination of nivolumab with ipilimumab (anti-CTLA-4) antibodies [7]. While providing 8 to 19.2 months of survival benefit [5], both resistance to these treatments and limited tolerability can lead to severe and, in some cases, unmanageable adverse events in HCC patients [5, 8–11]. Thus, there is a pressing clinical need for new targeted and potentially more tolerable therapies for the treatment of HCC.

Recent “multi-omics” data from 363 liver cancer patients from The Cancer Genome Atlas (TCGA) identified three integrative Cluster (iClust) HCC subtypes based on the integration of several molecular features, including transcript abundance, copy number and sequence variations, and DNA methylation [12]. Clinically, the iClust1 subtype comprises patients of younger age, female gender, and Asian ethnicity. These are high-grade tumors associated with macrovascular invasion and the worst survival outcomes. The iClust2 includes low-grade HCC with less microvascular invasion and overall better prognosis than the iClust1 and iClust3 subtypes. Lastly, iClust3 tumors exhibit higher frequencies of chromosomal instability, *TP53* mutations, and DNA hypomethylation throughout the genome. These genomic studies also highlighted potential tumor suppressor genes (TSGs) presenting DNA promoter hypermethylation concurrent with gene silencing. While some TSGs are

already known to play a key role in HCC pathogenesis, including the cell cycle regulator *CDKN2A* [12–14], some less well-characterized targets have been found selectively silenced in specific iClust HCC subtypes. However, the causative functional role of these TSGs during HCC pathogenesis remains unknown. Thus, genome engineering technologies able to specifically and selectively reactivate these TSGs could facilitate the functional interrogation of these loci as potential drivers of HCC. Importantly, these technologies also represent a new generation of precision oncology approaches for the personalized treatment of HCC.

Reactivation of TSGs has previously been achieved with inhibitors of epigenetic enzymes that either deposit silencing marks in the DNA and associated histones, such as DNA methyltransferases (DNMTs), including 5-aza-2'-deoxycytidine (decitabine), or that erase activating marks, such as histone deacetylases (HDACs), including suberoylanilide hydroxamic acid (vorinostat). However, potential limitations of these regimes include high toxicities after prolonged treatment, with the eventual development of drug resistance. These toxicities have been correlated with genome-wide effects due to the lack of locus selectivity of these treatments [15–17].

Clustered Regularly Interspaced Short Palindromic Repeats/CRISPR-associated protein 9 (CRISPR/Cas9) adapted for epigenetic editing represents an emerging technology to reactivate genes with high selectivity, thereby enabling functional interrogation of TSGs. In CRISPR-activation (CRISPRa) systems, a catalytically dead nuclease from *Streptococcus pyogenes*, *SpdCas9*, is fused to one or more activator domains or epigenetic effector domains (EDs). These fusions are directed or targeted to a genomic region by co-expression of a 20-nucleotide (nt) guide RNA (gRNA). This versatile system has been exploited for specific re-expression of several loci by expression of multiple gRNAs targeting different TSGs, such as *MASPIN* in lung cancer cells [18], *RPRM* in gastric cancer cells [18], *PTEN* in triple-negative breast cancer and melanoma [19], *DKK3* in prostate cancer [20], and *CCN6* in a mouse model of breast cancer [21].

In the context of HCC, CRISPR/Cas9 technologies have been employed for genome-scale knockout screens to identify TSGs, such as *ADAMTSL3* and *PTEN* [22]. Similarly, a CRISPRa screening library has enabled the identification of key drivers of sorafenib resistance, such as *PHGDH* [23] and *LRP8* [24]. However, to the best of our knowledge, CRISPRa platforms have not been adopted for rational and simultaneous targeting of multiple TSGs silenced in clinical specimens of HCC, particularly in the aggressive subtypes of HCC.

In this study, we bioinformatically analyzed a panel of 12 candidate TSGs (*BCO2*, *CDKN2A*, *CPS1*, *HHIP*,

miR-122-5p, *MT1E*, *MT1M*, *PSAT1*, *PTGR1*, *PZP*, *TMEM106A*, and *TTC36*) that are epigenetically silenced and under-expressed in HCC tumor samples compared to normal tissue. By investigating a panel of epigenetic effector domains and gRNAs, we demonstrate that CRISPRa systems strongly and selectively activate up to four different TSGs in representative HCC cell lines harboring hypermethylated and silenced genes. Comparison of the CRISPRa system with epi-drugs (decitabine and vorinostat) confirmed the superior locus selectivity of gRNA systems relative to currently approved epigenetic inhibitors. Our study outlines a customizable epigenetic editing toolkit to reactivate “at will” multiple candidate TSGs in HCC patients.

Results

Associations between RNA abundance, promoter DNA hypermethylation, and copy number variation identified a 12-tumor suppressor gene panel

To functionally interrogate multiple TSGs and in a wide range of HCC patients, we first performed an extended bioinformatic analysis of available data from The Cancer Genome Atlas (TCGA). A previous study identified eight genes exhibiting an inverse correlation between DNA methylation (DNAm) and gene expression in HCC patient’s specimens relative to matched normal control, with some of these genes encoding tumor-suppressive proteins [12]. These genes included *CDKN2A*, *CPS1*, *HHIP*, *MT1E*, *MT1M*, *PTGR1*, *TMEM106A*, and the most abundant hepatic miRNA, *miR-122-5p*. Importantly, integration of copy number variation, gene mutations, and DNAm identified three distinct integrative Clusters (iClust) of HCC patients, being iClust1 patients correlated with one of the poorest outcomes [12].

To pursue a more comprehensive approach, we utilized computational methods to infer the values of unspecified samples within the three iClusts, leading to the analysis of 357 tumor specimens, subdivided into iClust1 ($n=64$), iClust1-inf ($n=66$), iClust2 ($n=55$), iClust2-inf ($n=61$), iClust3 ($n=62$), and iClust3-inf ($n=49$) (Additional file 1: Fig. S1 and Additional file 12: Data S1). We also searched for additional genes with a strong inverse correlation between RNA abundance and DNAm levels within associated probes, and where the RNA abundance was generally higher within matched

normal tissue samples ($n=40$), where available (Additional file 13: Data S2, Additional file 14: Data S3). This analysis of 397 patients identified four additional candidate TSGs: *BCO2*, *PSAT1*, *PZP*, and *TTC36* (Fig. 1). Each gene captured subsets of patients within previously identified iClusters with evidence of reduced gene expression and promoter DNA hypermethylation relative to adjacent normal liver samples (*black markers*). Genes such as *BCO2* and *PZP* covered relatively large numbers of patients across all three subsets, while *TTC36*, *CPS1*, and *miR-122-5p* showed enrichment within subsets of iClust1 (*blue*), and lastly, *PSAT1* within subsets of iClust2 (*orange*) and iClust3 (*green*) patients.

While no individual gene showed evidence of DNA hypermethylation across all patients (Additional file 2: Fig. S2), and conversely, no individual patient showed promoter DNA hypermethylation across the full 12-gene panel, subsets of patients could be targeted by appropriate combinations, e.g., *BCO2*, *CDKN2A*, *PTGR1*, or *HHIP* for targeting iClust1 tumors; *CDKN2A*, *BCO2*, *PSAT1*, or *MT1E* for either iClust2 or iClust3 tumors; and *CDKN2A*, *PSAT1*, *MT1E*, or *TMEM106A* for iClust3 tumors (Additional file 2: Fig. S2). These data raise the possibility of augmenting the anticancer effect by creating “multiplexed” libraries of TSG reactivation constructs based on CRISPRa technology, thus achieving personalized therapy through tailored combinations of patient biomarkers.

Epigenetic inhibitors (epi-drugs) reactivate a subset of TSGs in the Hep3B and HuH-7 HCC cell lines

To validate the functional association between epigenetic regulation and transcriptional downregulation in the context of the 12-TSG gene panel, we investigated the effect of epi-drugs on mutually exclusive epigenetic marks such as DNAm and histone acetylation in representative HCC (Hep3B and HuH-7) cell lines. As observed in HCC clinical specimens, these lines demonstrated downregulation of several TSG’s mRNAs relative to non-transformed hepatocytes, particularly *HHIP*, *miR-122-5p*, *MT1E*, *MT1M*, *PZP*, and *TTC36* in Hep3B, and *HHIP*, *PZP*, *TMEM106A*, and *TTC36* in HuH-7 cells (Fig. 2A).

We subsequently treated both cell lines with clinically approved epigenetic inhibitors of DNA methyltransferases (DNMTs) and pan-histone deacetylases (HDACs)

(See figure on next page.)

Fig. 1 A 12-tumor suppressor gene panel from TCGA hepatocellular carcinoma patients shows gene silencing through promoter DNA methylation within subsets of liver cancer samples. **A** RNA transcript abundance (logTPM, z-score normalized), methylation of promoter-associated probes (β -value, z-score normalized), and copy number variation for the indicated genes (left to right), together with tumor sample “integrated-data cluster” (iClust) annotations. RNA abundance and DNA methylation are also shown for matched normal liver tissue samples where available. **B** Scatter plots showing the association between RNA transcript abundance (y-axis; logTPM) and associated probe-level of promoter DNAm (x-axis; β -value). Scatter markers colors correspond to adjacent normal liver (*black*), iClust1 (*blue*), iClust1-inf (*light blue*), iClust2 (*orange*), iClust2-inf (*light orange*), iClust3 (*green*), or iClust3-inf (*light green*) tumor samples. Further information on inferred iClusters (iClust-inf) is given in “Methods”

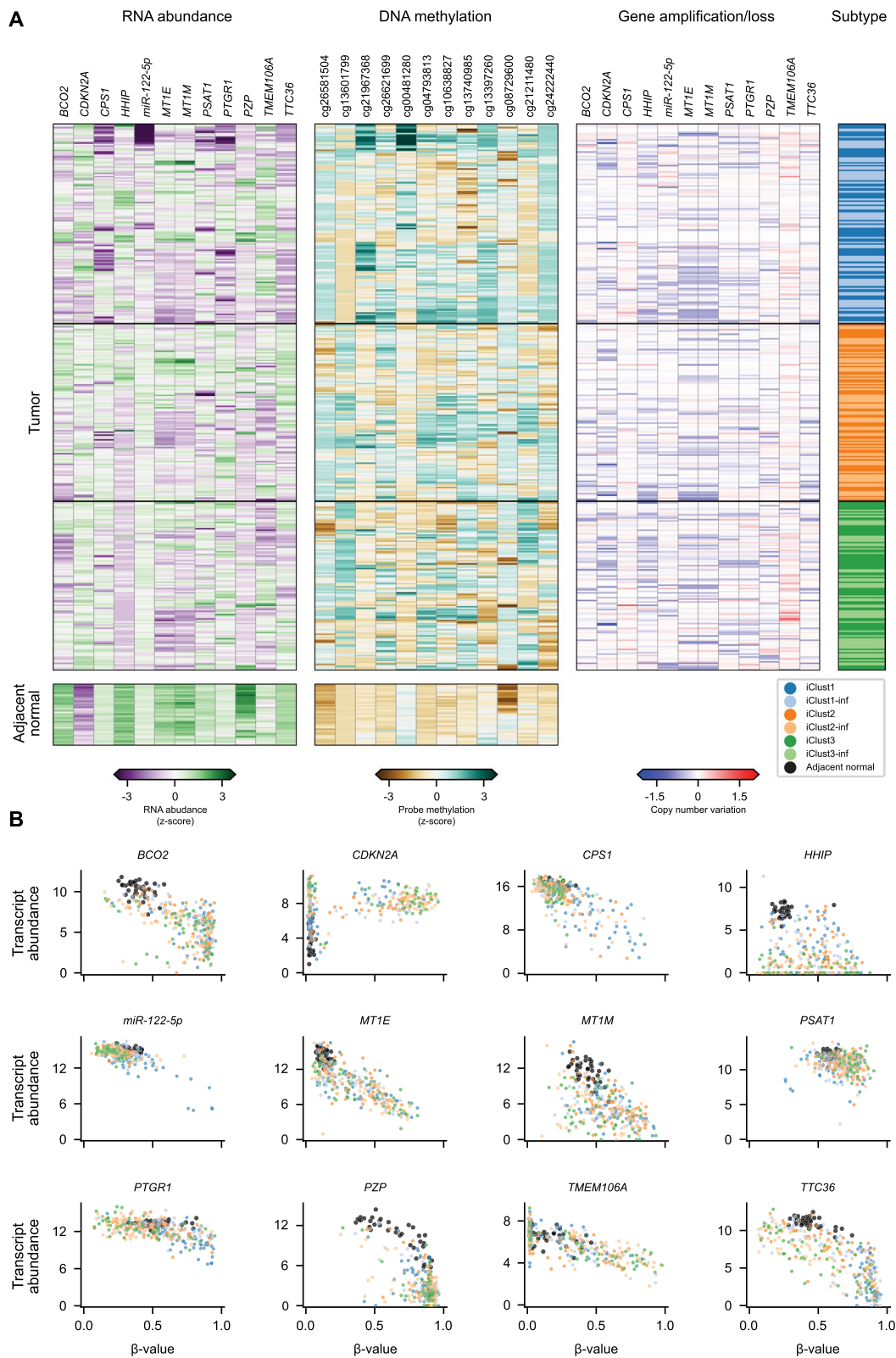


Fig. 1 (See legend on previous page.)

and monitored TSG expression by quantitative real-time PCR (qRT-PCR). The range of concentrations of 5-aza and SAHA and the duration of the treatments were selected to maximize gene upregulation while minimizing potential toxicities as reported in previous works [25–30]. As expected, pharmacological inhibition of DNMTs by decitabine (5-aza) or HDACs by vorinostat (SAHA) resulted in the reactivation of several TSGs. Treatment with 5-aza led to a significant de-repression of most TSGs in Hep3B cells (Fig. 2B) and, to a lesser extent, in HuH-7 cells (Fig. 2C), in accordance with the basal TSG mRNA abundance (Fig. 2A). This is also consistent with the bioinformatic analyses we performed on the available data, extracted from the Cancer Cell Line Encyclopedia (CCLE), of RNA abundance and DNAm (expressed as β -value) for Hep3B and HuH-7 cell lines (Additional file 3: Fig. S3).

In comparison with 5-aza, SAHA led to a lower but still significant degree of TSG mRNA upregulation. Furthermore, treatment with increasing concentrations of epigenetic inhibitors resulted in gene reactivation in a dose-dependent manner only for a subset of TSGs, including *BCO2*, *CDKN2A*, *HHIP*, *MT1E*, *MTIM*, *PTGR1*, and *PZP* (Fig. 2B–E). Unexpectedly, *CPS1* exhibited potent downregulation following treatment with 5-aza in both cell lines (Fig. 2B, C) or with SAHA in Hep3B (Fig. 2D). Similarly, *miR-122-5p* unexpectedly exhibited downregulation upon both treatments in HuH-7 cells (Fig. 2C, E).

Collectively, these data indicate that epi-drugs de-repress a subset of TSGs, albeit non-selectively. Moreover, unexpected significant transcriptional repression was observed for TSGs having basal levels of expression

in the aforementioned lines (Fig. 2A), such as *CPS1* and *miR-122-5p*.

CRISPR/SpdCas9-activation (CRISPRa) systems selectively reactivate TSGs in Hep3B and HuH-7 HCC cell lines

To investigate the focal and selective reactivation of individual TSGs, we exploited CRISPRa technology in a “hit-and-run” (transient transfection) approach. CRISPRa consists of the synergistic combination of *SpdCas9*, C-terminally fused to the tripartite transcriptional activator domain VPR (VP64, p65, and Rta) [31] with the gRNA-MS2-MCP (MS2-coat protein) which directs genomic specificity (Fig. 3A). This strategy enables the concomitant recruitment of the bipartite p65-HSF1 (heat shock factor 1) activator effector domains (EDs) [32] to the targeted genomic site.

For each TSG we designed four gRNAs targeting the proximal promoter and the nearby regulatory region mapping upstream and downstream of the transcription start site (TSS) (Additional file 10: Table S1). We focused on several candidate TSGs for each cell line having low or intermediate levels of basal expression relative to normal hepatocytes (Fig. 2A): *HHIP*, *MTIM*, *PZP*, *TTC36*, *MT1E*, *miR-122-5p*, and *PTGR1* in Hep3B cells (Fig. 3) and *HHIP*, *CPS1*, *PZP*, *TMEM106A*, *TTC36*, and *CDKN2A* in HuH-7 cells (Fig. 4). The gRNAs were selected based on established algorithms that predict both maximal on- and minimal off-target binding sites [33, 34] and qRT-PCR was performed 48 h post-transfection to quantitate mRNA expression; normal (non-transformed) human hepatocyte mRNA was processed as a reference control.

(See figure on next page.)

Fig. 2 Epi-drugs reactivate a subset of tumor suppressor genes in Hep3B and HuH-7 HCC cell lines. **A** Heatmap of the 12-tumor suppressor gene (TSG) panel comparing the mRNA expression in Hep3B and HuH-7 HCC cell lines versus normal hepatocytes. Gene expression was evaluated by qRT-PCR. Red color indicates the least expressed (cycle threshold 40) and blue color the highest expressed (cycle threshold 20) genes. Data are means ($n = 3$). **B, C** Transcriptional regulation of the 12-TSG panel 72 h after 5-aza treatment at different concentrations, indicated by color, in Hep3B and HuH-7 cells, respectively. The data show the fold log₁₀ change in TSG mRNA levels relative to vehicle-treated cells. From left to right, for Hep3B cells: *BCO2*: * $P = 0.000017, 0.000189, 0.000237, 0.000041, 0.000036$; *CDKN2A*: * $P = 0.001726, 0.000067, 0.000965, 0.000064, 0.000066$; *CPS1*: * $P = 0.000004, 0.000004, 0.000009, 0.000004, 0.000005$; *HHIP*: * $P = 0.001481, 0.032448, 0.003285$; *miR-122-5p*: * $P = 0.000884, 0.009364, 0.009338, 0.021386$; *MT1E*: * $P = 0.013894, 0.000860, 0.008483, 0.001014, 0.021049$; *MTIM*: * $P = 0.001025, 0.000295, 0.004843, 0.007027, 0.000230$; *PSAT1*: * $P = 0.011710, 0.020228, 0.004350$; *PTGR1*: * $P = 0.000021, 0.000004, 0.000007, 0.000130, 0.000010$; *PZP*: * $P = 0.000595, 0.018607, 0.000256, 0.006314$; *TMEM106A*: * $P = 0.000067, 0.000002, 0.000175, < 0.000001, 0.002216$; and *TTC36*: * $P = 0.003576, 0.001630, 0.001968, < 0.000001$. For HuH-7 cells: *BCO2*: * $P = 0.000234, 0.000074, 0.009780, 0.002345, 0.000073$; *CDKN2A*: * $P = 0.002474, 0.002569, 0.004410, 0.001787, 0.000041$; *CPS1*: * $P = 0.000012, 0.000018, 0.000023, 0.000031, 0.000052$; *HHIP*: * $P = 0.011967, 0.008680, 0.000309, 0.000009$; *miR-122-5p*: * $P = 0.002266, 0.001959, 0.002015, 0.001671, 0.002592$; *PSAT1*: * $P = 0.009506, 0.012759, 0.022472, 0.020526$; *PTGR1*: * $P = 0.008993, 0.000421, 0.002261, 0.000051$; *PZP*: * $P = 0.000718, 0.012523, 0.000963, 0.000180, 0.001813$; *TMEM106A*: * $P = 0.000001, 0.000003, 0.000603, 0.000005, 0.000717$; and *TTC36*: * $P = 0.012646, 0.000005, 0.002686, < 0.000001, 0.000026$. **D, E** Transcriptional regulation of the 12-TSG panel 48 h after SAHA treatment at different concentrations, indicated by color, in Hep3B and HuH-7 cells, respectively. The data show the fold log₁₀ change in TSG mRNA levels relative to vehicle-treated cells. From left to right, for Hep3B cells: *BCO2*: * $P = 0.000006, < 0.000001, 0.000511$; *CPS1*: * $P = 0.000209, 0.000020, 0.000003$; *HHIP*: * $P = 0.003836, 0.000015$; *MT1E*: * $P = 0.004923, 0.005036$; *MTIM*: * $P = 0.001981, 0.001938, 0.003620$; *PSAT1*: * $P = 0.000809$; *PTGR1*: * $P = 0.000052, 0.000013, 0.000023$; *TMEM106A*: * $P = 0.001558, 0.002973$; and *TTC36*: * $P = 0.000448$. For HuH-7 cells: *BCO2*: * $P = 0.000019, 0.000023, 0.000054$; *CDKN2A*: * $P = 0.000785, 0.000030, 0.000190$; *CPS1*: * $P = 0.000156, < 0.000001$; *HHIP*: * $P = 0.005756$; *miR-122-5p*: * $P = 0.000968, 0.001295$; *MT1E*: * $P = 0.002001$; *PTGR1*: * $P = 0.000127$; and *TMEM106A*: * $P = 0.000221, 0.001073, 0.001910$. The data presented as means \pm SEM ($n = 3$), and P values were determined by multiple unpaired t -test comparisons with a two-stage linear step-up procedure of Benjamini, Krieger, and Yekutieli

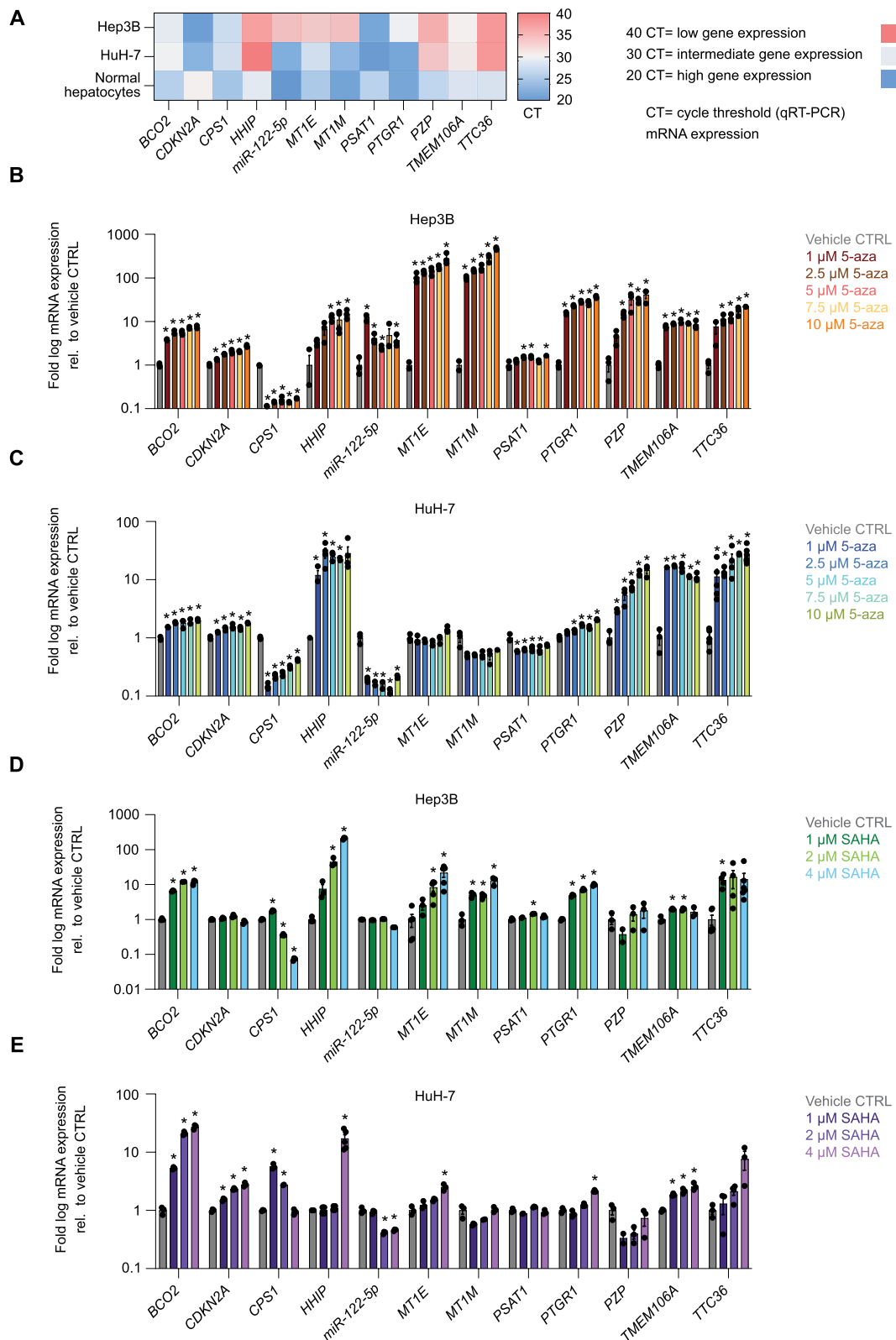


Fig. 2 (See legend on previous page.)

We observed significant CRISPRa-mediated transcriptional upregulation of all the TSGs targeted relative to the empty vector control (EV) or to CRISPRa in absence of gRNA (NO G). However, the activation of TSGs achieved by CRISPRa in HCC lines partially reached the physiological mRNA levels expressed in normal hepatocytes (Figs. 3, 4). Notably, one specific gRNA was sufficient to attain the strongest gene reactivation for most of the TSGs examined, as in the case for *HHIP* (gRNA 4 (G4) vs. EV, 349.5-fold, $P < 0.0001$), *MTIM* (G1, 10,211-fold, $P < 0.0001$), *PZP* (G2, 145.3-fold, $P < 0.0001$), *TTC36* (G3, 50.6-fold, $P = 0.0001$), *MT1E* (G1, 11.45-fold, $P < 0.0001$), *miR-122-5p* (G2, 1.4-fold, $P = 0.0014$), and *PTGR1* (G2, 6.0-fold, $P < 0.0001$) in Hep3B cells (Fig. 3B–H). A similar pattern was observed in HuH-7 cells for *PZP* (G2 vs. EV, 4,500-fold, $P < 0.0001$), *TTC36* (G3, 265.6-fold, $P < 0.0001$), *CPS1* (G1, 6.7-fold, $P < 0.0001$), and *TMEM106A* (G1, 5.8-fold, $P < 0.0001$, nearly as much as the MIX 4G, 6.2-fold, $P < 0.0001$) (Fig. 4B–E). For *HHIP* and *CDKN2A* in HuH-7 cells, the combinations of all designed gRNAs (MIX) were necessary to maximize TSG activation, i.e., the mix of four guides (MIX 4G vs. EV, 13,852-fold, $P < 0.0001$) (Fig. 4A), and the mix of five guides (MIX 5G, 1.95-fold, $P < 0.0001$) (Fig. 4F), respectively. Importantly, CRISPRa enabled all the targeted TSGs to be upregulated relative to EV or NO G controls, despite their basal gene expression, in contrast to the epi-drugs, which led to unexpected downregulation of some TSGs, such as *CPS1* and *miR-122-5p*.

Moreover, CRISPRa outperformed the epi-drug treatments (5-aza or SAHA, all concentrations tested) in upregulating *HHIP*, *MTIM*, *PZP*, *TTC36*, and *CPS1*, whereas 5-aza, but not SAHA led to a higher activation of *MT1E*, *miR-122-5p*, *PTGR1*, and *TMEM106A* compared to CRISPRa. Only the highest doses of SAHA (2 and 4 μM) exceeded CRISPRa-based upregulation of *PTGR1* and *CDKN2A* (Additional file 15: Data S4).

To investigate unintended gene modulation by CRISPRa, we bioinformatically analyzed the most active gRNA sequences, for each of the ten targeted TSGs, for

genome-wide mismatches equal to or less than three mispairs [35]. We, then, matched the genomic location of the putative gRNA off-target binding sites in the human genome browser to identify those in the proximity of genomic regulatory elements, i.e., promoters and enhancers. Next, qRT-PCR was conducted on the potential off-targets to assess their transcriptional regulation by CRISPRa (Additional file 4, 5: Fig. S4 and Additional file 16: Data S5). We found no significant gene modulation of any of the bioinformatically predicted (potential) off-target genes, consistently with previous works [36], suggesting negligible off-target activities.

SpdCas9-VPR and MS2-MCP-p65-HSF1 is the most potent CRISPRa platform for “hit-and-run” TSG reactivation

Since our most downregulated TSGs were marked by DNAm (Additional file 3: Fig. S3), we next investigated whether the DNA demethylase catalytic domain (CD) of TET1, Ten-Eleven Translocation methylcytosine dioxygenase 1, could be exploited to reactivate these genes. We chose *HHIP*, *PZP*, and *TTC36* in Hep3B and HuH-7 cells as well as *MTIM* in Hep3B cells, since these targets had the lowest transcript levels (Fig. 2A), resulting in a strong re-expression upon epi-drug treatment, particularly with 5-aza (Fig. 2B, C), and also given the strong negative correlation between their RNA abundance and DNAm status observed in patients (Fig. 1) as well as in Hep3B and HuH-7 cell lines (Additional file 3: Fig. S3). Furthermore, to identify additional (potentially synergistic) combinatorial strategies for TSG reactivation, we combined TET1-CD and MS2-MCP-TET1-CD with the epigenetic editors VPR and MS2-MCP-p65-HSF1 comprising a compact “epi-toolbox” of eight different CRISPRa (Fig. 5A). Unexpectedly, TET1-CD alone, either tethered to *SpdCas9*, or recruited by the MS2-MCP system, or even concomitantly fused and recruited, was unable to de-repress any of the TSGs targeted in either of the two HCC lines transiently transfected along with the most potent gRNA/s or with no gRNA as control (Fig. 5B–H). Similarly, there were no changes in *MTIM* nor in *TTC36* mRNA

(See figure on next page.)

Fig. 3 Upregulation of tumor suppressor genes by CRISPRa in Hep3B HCC cells. **A** Schematic representation of CRISPRa consisting of *SpdCas9* C-terminally fused to the tripartite transactivator VPR (VP64, p65, and Rta) and coupled with the gRNA-MS2-MCP system that recruits the bipartite transactivator p65-HSF1 for targeted epigenetic editing. As indicated for each tumor suppressor gene (TSG), gRNAs, designated as G1, G2, G3, and G4, direct CRISPRa to the forward (right arrow) or reverse (left arrow) DNA strand within the regulatory region and proximal promoter of the TSG. gRNA numbering (\pm) refers to the distance in base pairs from the transcription start site (TSS) of each targeted TSG. **B–H** Reactivation of TSGs by CRISPRa was evaluated by qRT-PCR 48 h after transient transfection. Fold change in TSG mRNA expression from transfected cells with CRISPRa and TSG-targeting gRNAs, and normal hepatocytes was normalized to control transfections with empty vector (EV) and compared to CRISPRa with no gRNA (NO G) for statistical analysis. From left to right: **B** *HHIP*: $*P = 0.0390$, $****P < 0.0001$; **C** *MTIM*: $***P = 0.0004$, $****P < 0.0001$; **D** *PZP*: $***P = 0.0006$, $****P < 0.0001$, $***P = 0.0002$, $*P = 0.0359$, $**P = 0.0013$, $****P < 0.0001$; **E** *TTC36*: $**P = 0.0013$, $**P = 0.0022$, $***P = 0.0001$, $****P = 0.0004$, $****P < 0.0001$; **F** *MT1E*: $*P = 0.0349$, $****P < 0.0001$, $***P = 0.0002$; **G** *miR-122-5p*: $**P = 0.0014$, $*P = 0.0119$, $****P < 0.0001$; **H** *PTGR1*: $****P = 0.0001$, $****P < 0.0001$. Data presented as means \pm SEM ($n = 3$), and P values were determined by unpaired t -test. *SpdCas9* *Streptococcus pyogenes* deactivated Cas9 protein adopted for epigenome engineering, MS2 RNA aptamer, MCP MS2 coat protein, HSF1 heat shock factor 1, Chr chromosome, (+) forward DNA strand, (–) reverse DNA strand, and MIX 4G combination of all four gRNAs targeting a TSG

Hep3B

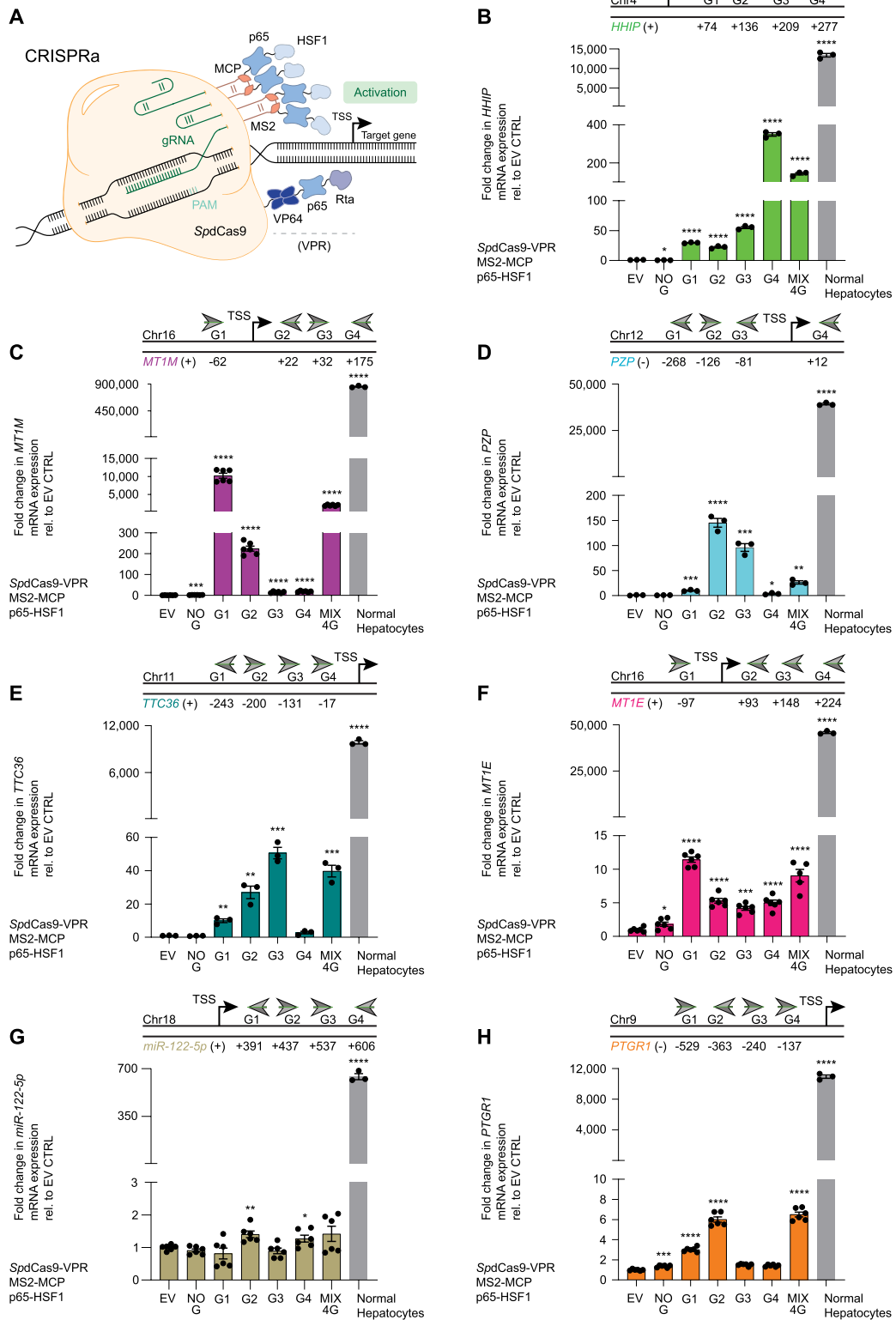


Fig. 3 (See legend on previous page.)

expression when tiling their respective gene promoters by a mix of four gRNAs directing *SpdCas9*-TET1-CD, or *SpdCas9*-TET1-CD in combination with MS2-MCP-TET1-CD in Hep3B cells (Additional file 6: Fig. S5). Instead, this combinatorial approach underscored the significant superiority of *SpdCas9*-VPR synergistically combined with the MS2-MCP-p65-HSF1 system in reactivating all four highly downregulated targeted TSGs (*HHIP*, *MT1M*, *PZP*, and *TTC36*) in the respective cell lines (Fig. 5B–H). A synergistic booster effect was obtained when the tripartite (VPR) and the bipartite (p65-HSF1) activators were co-delivered.

Interestingly, the combinations consisting of *SpdCas9*-VPR with MS2-MCP-TET1-CD, and *SpdCas9*-TET1-CD with MS2-MCP-p65-HSF1, also exhibited a significant gene reactivation of all four targeted TSGs, apart from *HHIP* in Hep3B cells targeted by the former (Fig. 5B–H).

To ascertain the functional association between DNAm and the observed *HHIP* re-expression (150-fold, $P < 0.0001$) achieved by *SpdCas9*-TET1-CD, MS2-MCP-p65-HSF1, and gRNA G4, we performed DNAm analyses (Infinium Methylation EPIC 850K arrays) in Hep3B cells transiently transfected for 96 h (Additional file 7: Fig. S6). Surprisingly, we found no significant targeted DNA demethylation in the *HHIP* proximal promoter, nor for the most potent CRISPRa (*SpdCas9*-VPR and MS2-MCP-p65-HSF1) guided by the same gRNA G4, which does not engage TET1-CD, but that nevertheless led to the highest *HHIP* re-expression (781-fold, $P < 0.0001$) (Additional file 7: Fig. S6 and Additional file 17: Data S6). Furthermore, no significant genome-wide changes in DNAm were detected for these two CRISPRa transfected conditions, relative to NO G controls.

Since TET1-CD, either fused to *SpdCas9* and/or recruited by the gRNA-MS2-MCP-system, did not lead to significant TSG reactivation in transiently transfected cells, we next investigated an “all-in-one” lentiviral vector which enabled the generation of stable cell lines constitutively co-expressing the gRNA along with *SpdCas9*-TET1-CD. When the *SpdCas9*-TET1-CD construct was co-expressed with a mix of four gRNAs targeting *HHIP* in Hep3B cells, no significant upregulation was observed relative to NO G control, even 40 days after transduction of the cells, nor in the context of *MT1M* targeted by four single gRNAs (G1, G2, G3, and G4) or their mix, 20 days post-transduction. In contrast,

SpdCas9-VPR led to a robust *MT1M* gene de-repression in Hep3B cells (G1 vs. NO G, 17,382-fold, $P < 0.0001$) (Additional file 8: Fig. S7).

Overall, these results suggest that *SpdCas9*-VPR synergistically combined with the MS2-MCP-p65-HSF1 recruiting system, or the *SpdCas9*-VPR alone are the most effective CRISPRa platforms for the reactivation of several highly silenced TSGs in HCC cells.

CRISPRa reactivates TSGs more specifically and more potently than epi-drugs and enables genome multiplexing “at will”

We next compared the specificity and the potency of CRISPRa technologies versus traditional epi-drug-based inhibition (decitabine and vorinostat) for the reactivation of TSGs in “hit-and-run” approaches (transient transfection of CRISPR vectors *SpdCas9*-VPR and MS2-MCP-p65-HSF1). To this aim, we focused on the most downregulated TSGs (*HHIP*, *MT1M*, *PZP*, and *TTC36*) in Hep3B (Fig. 6A–C) and *HHIP*, *PZP*, and *TTC36* in HuH-7 (Fig. 6D–F). Cells were either transfected with an optimized CRISPRa (*SpdCas9*-VPR and MS2-MCP-p65-HSF1) platform and single gRNA targeting either single TSGs, or by combining multiple gRNAs to assess the efficacy of TSG multiplexing. Fold-transcriptional changes were cross-examined by qRT-PCR, and data were normalized and visualized in heatmap plots relative to NO G control. In contrast to 5-aza and SAHA, which caused uncontrolled concurrent reactivation of several TSGs relative to vehicle control, CRISPRa platforms demonstrated a high degree of on-target specificity in both cell lines, with non-detectable off-target effects. Notably, the degree of non-specific TSG reactivation induced by the epi-drugs depended on the nature of the inhibitor used (with 5-aza being stronger than SAHA) and varied upon the concentrations utilized. Additionally, by comparing the fold-change in cognate mRNA regulation achieved between CRISPRa technology (Fig. 6A, D) with those of the epi-drug treatments (Fig. 6C, F), we observed higher activation of CRISPRa systems by several orders of magnitude relative to the conventional inhibitors in de-repressing individual TSGs. The fold changes obtained were dependent on the type of the epi-drug and the concentrations utilized, as well as the target gene, and it is cell-type specific (Additional file 15: Data S4). Importantly, even when performing up to 4-TSG multiplexing,

(See figure on next page.)

Fig. 4 Upregulation of tumor suppressor genes by CRISPRa in HuH-7 HCC cells. **A–F** Reactivation of TSGs by CRISPRa was evaluated by qRT-PCR 48 h after transient transfection. Fold change in TSG mRNA expression from transfected cells with CRISPRa and TSG-targeting gRNAs, normal and immortalized hepatocytes was normalized to control transfections with empty vector (EV), and compared to CRISPRa with no gRNA (NO G) for statistical analysis. From left to right: **A** *HHIP*: **** $P < 0.0001$; **B** *CP51*: **** $P < 0.0001$, *** $P = 0.0005$; **C** *PZP*: **** $P < 0.0001$; **D** *TMEM106A*: **** $P < 0.0001$, ** $P = 0.0063$; **E** *TTC36*: *** $P = 0.0001$, **** $P < 0.0001$, *** $P = 0.0003$; **F** *CDKN2A*: *** $P = 0.0010$, * $P = 0.0185$, **** $P < 0.0001$. Data presented as means \pm SEM ($n = 3$), and P values were determined by unpaired t -test

HuH-7

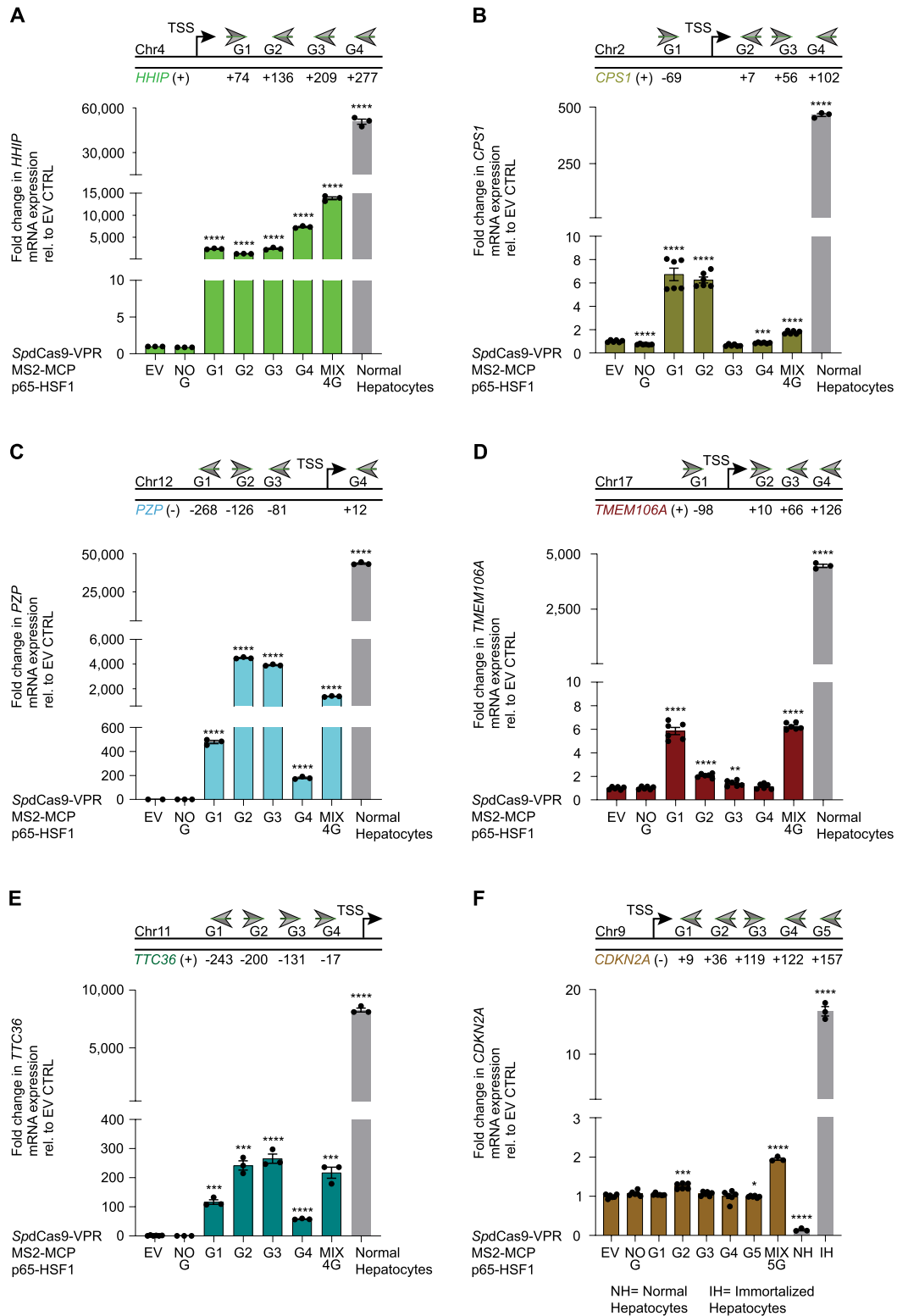


Fig. 4 (See legend on previous page.)

the fold changes achieved in TSG mRNA regulation employing CRISPRa were significantly higher than those observed with the epi-drugs (Fig. 6B–C, E–F).

Taken together, these data demonstrate that CRISPRa enabled at command “genome multiplexing,” facilitating the simultaneous reactivation of up to four TSGs, and reaching significantly higher levels of activation than those obtained with the epi-drugs for most of the TSGs targeted (Additional file 15: Data S4).

Reactivation of TSGs, either individually or in combination, via CRISPRa, reduces HCC cell proliferation, cell viability, and cell migration

We next investigated whether the reactivation of TSGs targeted individually and/or multiplexed by CRISPRa technology led to associated phenotypic cell reprogramming of HCC cells. To bypass the high cell-to-cell phenotypic variability reported in transient transfection assays due to a large number of plasmids transfected as well as the heterogeneous sizes (gRNA vs. *SpdCas9*-VPR) of the plasmids, we generated stable, lentivirally transduced, Hep3B cell lines. These transduced cells constitutively expressed the “all-in-one” lentiviral vector encoding *SpdCas9*-VPR and the most potent gRNA for each targeted TSG (Fig. 7). We focused on the four highly silenced TSGs: *HHIP*, *MT1M*, *PZP*, and *TTC36* in Hep3B cells. As shown in Fig. 7A, B, we achieved potent TSG re-expression by targeting the four TSGs, either individually (*HHIP*, G4 vs. NO G, 883-fold, $P < 0.0001$; *MT1M*, G1, 57,534-fold, $P < 0.0001$; *PZP*, G2, 1,541-fold, $P < 0.0001$; and *TTC36*, G3, 856-fold, $P < 0.0001$), or as 4-gene multiplexing (MIX 4 genes) by simultaneously co-delivering multiple gRNAs (*HHIP*, G4 vs. NO G, 121-fold, $P < 0.0001$; *MT1M*, G1, 8,745-fold, $P < 0.0001$; *PZP*, G2, 167-fold, $P < 0.0001$; and *TTC36*, G3, 55-fold, $P = 0.0107$). Similar to transient systems, we observed no significant cross-gene modulation within the four targeted TSGs (Fig. 7B) nor in the bioinformatically identified potential off-target genes (Additional file 4, 5: Fig. S4), outlining the high specificity of CRISPRa technology, even with constitutively expressed lentiviral vectors.

Immunofluorescence assays of the transduced cells demonstrated that *SpdCas9*-VPR was expressed mainly in the nucleus of the Hep3B cells, whereas *HHIP* was detected in the nucleus and plasma membrane. The *MT1M* and *TTC36* targets showed nuclear localization, and *PZP* was predominantly found in the extracellular space and plasma membrane as well as in the cytoplasm (perinuclear). These data show that the TSG mRNA upregulation achieved by CRISPRa was sufficient to elicit changes in expression at protein level, even for targets that were mostly silenced in control cells with undetectable protein levels, such as *MT1M*. Importantly, all these 4 co-targeted TSGs were found upregulated in the multiplexing (MIX 4 genes) condition, outlining the efficiency of CRISPRa in reactivating multiple targets at once (Fig. 7C–F).

To correlate the extent of TSG re-expression with cancer cell phenotypic remodeling, Hep3B cells transduced with *SpdCas9*-VPR targeting *HHIP* or the multiplexed four TSGs (*HHIP*, *MT1M*, *PZP*, and *TTC36*) were processed by cell proliferation, cell viability, and cell migration assays. We observed a significant decrease in the expression of the proliferative marker Ki-67 by 18% for *HHIP* G4 ($P < 0.0001$) and by 13% for MIX 4 genes ($P = 0.0003$), compared to *SpdCas9*-VPR NO G (Fig. 7G). Similarly, the impact on tumor cell viability over 72 h was found more pronounced upon targeting *HHIP* with G4 alone ($P < 0.0001$), although still significantly lessened in the MIX 4 genes condition ($P < 0.0001$) relative to NO G control (Fig. 7H). These analyses demonstrated that *HHIP* was a key TSG controlling liver cancer cell proliferation and cell viability; in fact, only modest changes in cell viability were achieved when individually targeting *MT1M*, *PZP*, and *TTC36* (Additional file 9: Fig. S8).

Interestingly, there was a significant reduction (77%, ~40%, and 20%) in migratory cells in the *TTC36* G3, in the MIX 4 genes, and in the *HHIP* G4 conditions, respectively, vs. NO G control ($P < 0.0001$, $P = 0.0008$, $P = 0.0390$) (Fig. 7I), whereas neither *MT1M* G1 nor *PZP* G2 conditions perturbed the migratory capacity in

(See figure on next page.)

Fig. 5 Maximizing reactivation of highly downregulated tumor suppressor genes in Hep3B and HuH-7 HCC cells. **A** Schematic representation depicting the CRISPRa toolbox developed for epigenetic editing. *SpdCas9* C-terminally fused to VPR, i.e., *SpdCas9*-VPR (dark blue); gRNA-MS2-MCP-p65-HSF1 recruiting system (light blue); *SpdCas9* C-terminally fused to TET1 catalytic domain, i.e., *SpdCas9*-TET1-CD (dark pink); gRNA-MS2-MCP-TET1-CD recruiting system (light pink); and *SpdCas9* (yellow). **B–H** Fold change in *MT1M* (**B**), *HHIP* (**C, D**), *PZP* (**E, F**), and *TTC36* (**G, H**) mRNA expression evaluated by qRT-PCR 96 h after transient transfection in Hep3B and HuH-7 cells. Cells were transfected with combinations of CRISPRa along with the most potent tumor suppressor gene-targeting gRNA/s, or with no gRNA (NO G) as control. Relative gene expression was normalized and compared to cells transfected with empty vector control (EV) for statistical analysis. From left to right: **B** *MT1M*: **** $P < 0.0001$, *** $P = 0.0002$; **C** *HHIP*: **** $P < 0.0001$, *** $P = 0.0008$; **D** *HHIP*: **** $P < 0.0001$, *** $P = 0.0002$; **E** *PZP*: *** $P = 0.0002$, **** $P < 0.0001$, ** $P = 0.0022$, *** $P = 0.0003$, *** $P = 0.0001$; **F** *PZP*: **** $P < 0.0001$; **G** *TTC36*: **** $P < 0.0001$, * $P = 0.0190$, ** $P = 0.0030$; **H** *TTC36*: **** $P < 0.0001$, ** $P = 0.0088$, *** $P = 0.0007$. Data presented as means \pm SEM ($n = 3$), and P values were determined by unpaired t -test. *SpdCas9* *Streptococcus pyogenes* deactivated Cas9 protein adopted for epigenome engineering, VPR VP64, p65, Rta, MS2 RNA aptamer, MCP MS2-coat protein, HSF1 heat shock factor 1, TET1-CD Ten-Eleven Translocation methylcytosine dioxygenase 1-catalytic domain, MIX 4G combination of four gRNAs

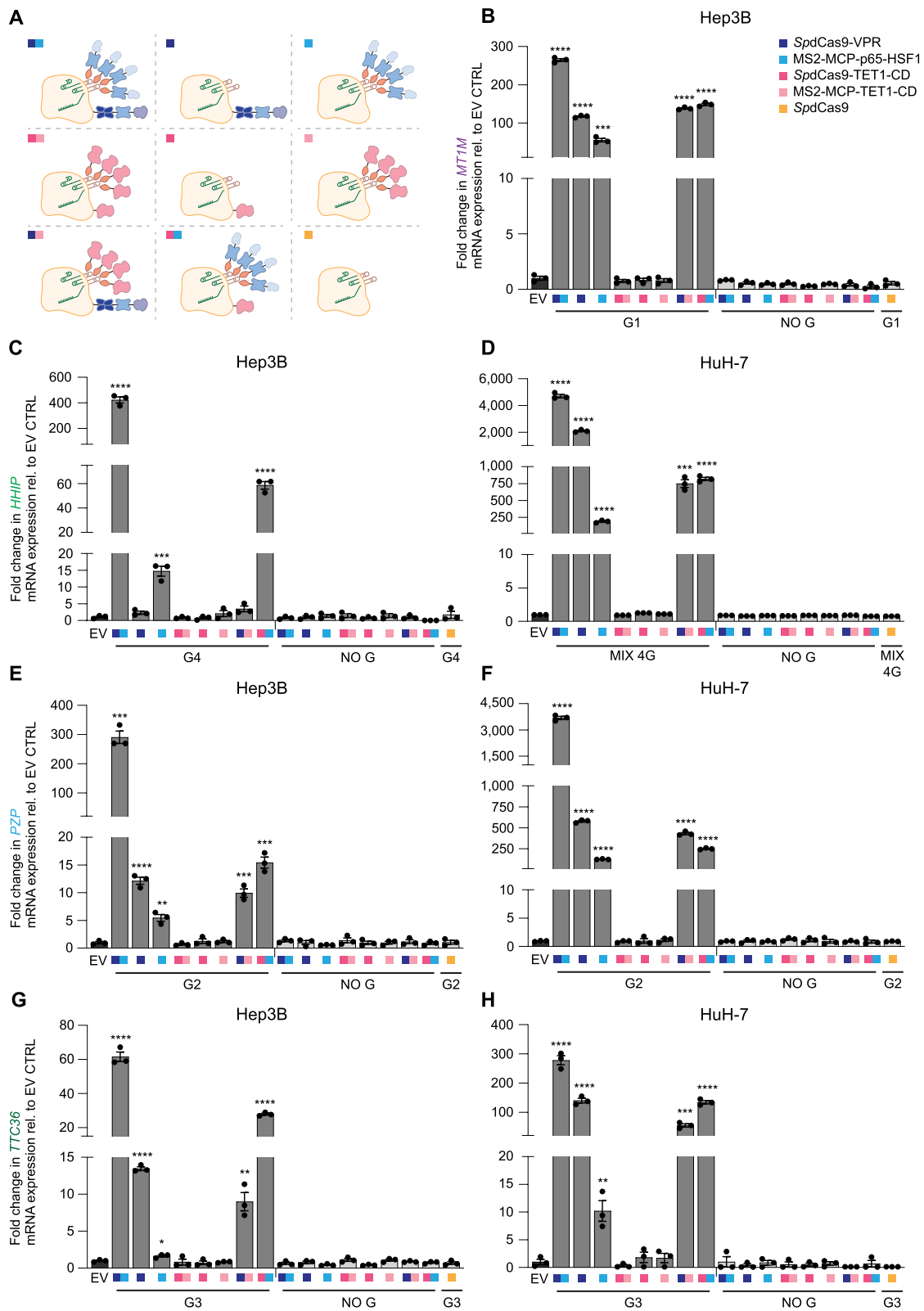


Fig. 5 (See legend on previous page.)

the respective stable Hep3B cell lines (Additional file 9: Fig. S8).

In conclusion, these data demonstrate that CRISPRa is a potent and highly specific platform to interrogate the functional role of silenced TSGs. We also demonstrate that multiplexing of various TSGs facilitates the functional regulation of various facets of TSG biology at once, in this case, regulation of cell growth and migration, making it a promising precision oncology tool for the treatment of liver cancer.

Discussion

We have developed a CRISPRa toolbox of epigenetic effector domains and gRNAs for the targeting of single and multiple combinations of TSGs in HCC cells. This approach could be harnessed for the functional interrogation of TSGs, and, ultimately, as a precision medicine for the treatment of aggressive forms of HCCs. These patients have few treatment options, and their clinical benefit is limited, particularly for late-stage HCC, as they often develop resistance.

Our computational analysis validated a 12-gene TSG panel which comprehensively captures all available HCC patients across the three main integrative clusters (iClusts) of HCC. These TSGs are both downregulated at the mRNA level and marked by DNA promoter methylation in clinical cohorts of HCC patients. We demonstrated that the CRISPRa approach represents a versatile toolkit to multiplex TSGs with high precision, potentially representing innovative tailored treatments for the different subtypes of HCC.

Our 12-gene TSG panel comprises: (1) regulators of cell cycle, e.g., *CDKN2A* [13, 14]; (2) metabolic enzymes such as *BCO2* [37, 38] (a regulator of lycopene metabolism), *CPS1* [39] (a liver-specific, intramitochondrial, rate-limiting enzyme in the urea cycle), *PTGR1* [40] (a bifunctional enzyme that inactivates leukotrienes and prostaglandins), and *PSATI* [41, 42] (a phosphoserine aminotransferase); (3) regulators of stemness, such as *HHIP* [43–49], which is a suppressor of the Hedgehog signaling pathway involved in embryonic development and tumorigenicity; (4) pro-apoptotic factors including the metallothioneins *MTIE* [50, 51] and *MTIM* [52–54], which act as a surveillance systems for carcinogens-caused cellular damage; immune-regulators, such as the transmembrane protein *TMEM106A* [55, 56] (an activator of the MAPK and NF- κ B signaling pathways implicated in the pro-inflammatory and anti-tumoral M1-type macrophage polarization); and (5) negative regulators of migration, invasion, angiogenesis, and metastasis, such as the liver specific *miR-122-5p* [57, 58] (a post-transcriptional regulator of genes involved in TNF and Notch signaling pathways), *PZP* [59–61] (a proteinase inhibitor), and *TTC36* [62–64] (a regulator of the Wnt- β -catenin pathway). Thus, while we focused on a limited array of phenotypic assays, the multiplexing approach has great potential to reprogram multiple aspects of HCC pathobiology, which could potentially facilitate a more comprehensive and multifactorial reprogramming of the HCC phenotype, including the tumor microenvironment.

To activate the array of 12 TSGs, we investigated CRISPRa platforms combining different gRNAs and

(See figure on next page.)

Fig. 6 Specific and potent reactivation of silenced tumor suppressor genes by CRISPRa compared to epi-drugs, and CRISPRa-enabled genome multiplexing in Hep3B and HuH-7 HCC cells. **A–F** Heatmap of the 12-tumor suppressor gene (TSG) panel comparing the fold change in mRNA regulation evaluated by qRT-PCR 48 h after transient transfections (**A**), (**B**), (**D**) and (**E**), 72 h after 5-aza, or 48 h after SAHA treatments (**C**) and (**F**). The transfection conditions and the epi-drug treatments are arranged in rows, and the genes in columns. Hep3B and HuH-7 cells were either transfected with CRISPRa (*SpdCas9-VPR* and *MS2-MCP-p65-HSF1*) along with the most potent TSG-targeting gRNA, or with no gRNA (NO G) as control; or treated with epi-drugs or vehicle control. Relative gene expression was normalized to cells transfected with empty vector control and compared to CRISPRa with NO G (**A**), (**B**), (**D**), and (**E**), or normalized and compared to cells treated with vehicle control (**C**) and (**F**) for statistical analysis. Data presented as means ($n=3$). **A** Targeted transcriptional regulation of four TSGs by CRISPRa in Hep3B cells. *P* values were determined by two-way ANOVA with Dunnett's multiple comparisons test (*HHIP* G4: **** $P < 0.0001$; *MT1M* G1: **** $P < 0.0001$; *PZP* G2: **** $P < 0.0001$; and *TTC36* G3: **** $P < 0.0001$). **B** Targeted genome multiplexing for simultaneous transcriptional reactivation of four TSGs by CRISPRa in Hep3B cells. *P* values were determined by two-way ANOVA with Šidák's multiple comparisons test (*HHIP*: ** $P = 0.0092$; *MT1E*: *P* = not significant; *MT1M*: **** $P < 0.0001$; *PZP*: **** $P < 0.0001$; and *TTC36*: **** $P < 0.0001$). **C** Untargeted transcriptional regulation of several TSGs in Hep3B cells treated with 10 μ M 5-aza (*MT1E*: **** $P < 0.0001$; *MT1M*: **** $P < 0.0001$; *PTGR1*: **** $P < 0.0001$; *PZP*: **** $P < 0.0001$; and *TTC36*: * $P = 0.0207$), 1 μ M SAHA, or 4 μ M SAHA (*HHIP*: **** $P < 0.0001$; and *MT1E*: ** $P = 0.0089$). *P* values were determined by two-way ANOVA with Dunnett's multiple comparisons test. **D** Targeted transcriptional regulation of three TSGs by CRISPRa in HuH-7 cells. *P* values were determined by two-way ANOVA with Šidák's multiple comparisons test. (*HHIP* G4: **** $P < 0.0001$; *PZP* G2: **** $P < 0.0001$; and *TTC36* G3: **** $P < 0.0001$). **E** Targeted genome multiplexing for simultaneous transcriptional reactivation of three TSGs by CRISPRa in HuH-7 cells. *P* values were determined by two-way ANOVA with Šidák's multiple comparisons test (*HHIP*: **** $P < 0.0001$; *MT1E*: *P* = not significant; *PZP*: **** $P < 0.0001$; *TMEM106A*: *P* = not significant; and *TTC36*: **** $P < 0.0001$). **F** Untargeted transcriptional regulation of several TSGs in HuH-7 cells treated with 10 μ M 5-aza (*HHIP*: **** $P < 0.0001$; *PZP*: **** $P < 0.0001$; *TMEM106A*: **** $P < 0.0001$; and *TTC36*: **** $P < 0.0001$), 1 μ M SAHA, or 4 μ M SAHA (*BCO2*: **** $P < 0.0001$; *HHIP*: **** $P < 0.0001$; and *TTC36*: ** $P = 0.0072$). *P* values were determined by two-way ANOVA with Dunnett's multiple comparisons test

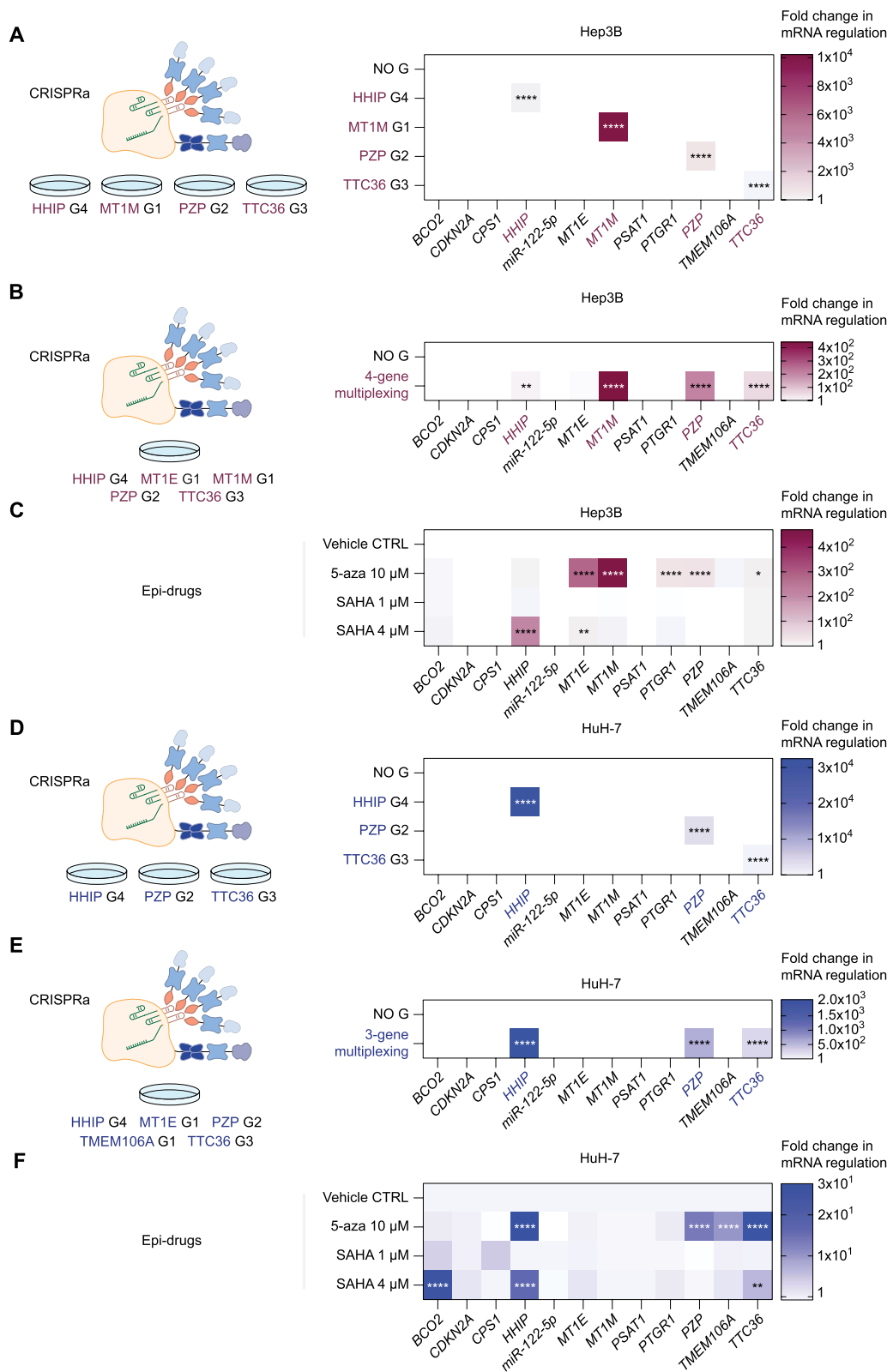


Fig. 6 (See legend on previous page.)

effector domains. In contrast to epigenetic drugs (decitabine and vorinostat) that led to a non-selective transcriptional modulation, we showed that CRISPRa systems enabled specific reactivation of single and multiple TSGs with negligible off-target effects, and were more potent in upregulating the majority of the TSGs targeted in the conditions tested in this study. The most silenced TSGs, including *HHIP*, *MT1M*, *PZP*, and *TTC36* were consistently reactivated by *SpdCas9*-VPR and MS2-MCP-p65-HSF1 epigenetic editing tools in both HCC cell lines tested in a hit-and-run (transient transfection) approach. This is consistent with our previous study on the TSGs *MASPIN* and *RPRM* in breast and gastric cancer cells [18].

While we did not observe reactivation in any of the four strongly silenced TSGs targeted by employing a DNA demethylase catalytic domain (TET1-CD), neither fused to *SpdCas9* and/nor recruited by the gRNA-MS2-MCP system, significant TSG reactivation was achieved when the TET1-CD was combined with other effectors, such as VPR or p65-HSF1. Similarly, *SpdCas9*-TET1-CD did not elicit significant TSG re-expression in the context of lentivirally transduced cells, neither by four individual gRNAs targeting *MT1M* nor by tiling *MT1M* or *HHIP* promoters with the mixture of four gRNAs. These findings are in contrast to previous works showing that TET1-CD fused to *SpdCas9* and/or recruited by the gRNA-MS2-MCP system enabled re-expression of TSGs, such as *BRCA1* in breast and cervical cell lines [65]; *SARI* in colon cancer [66]; *RANKL* [67] in neuroblastoma; several hypermethylated genes in lung adenocarcinoma, via the SunTag platform recruiting TET1-CD and VP64 [68]; and *FMRI* in induced pluripotent stem cells derived from fragile X syndrome patients by *SpdCas9*-TET1-CD encoded in a lentiviral vector [69]. Moreover, pioneering studies employing retroviral transduction

of Zinc-finger proteins engineered with TET-2-CD have shown reactivation of candidate TSGs, such as *C13ORF18* and *TFPI2* in cervical cancer cells [70], and *ICAM-1* in ovarian cancer cells [71].

Finally, we did not observe DNA demethylation changes upon *HHIP* reactivation in any of the CRISPRa epigenetic tools employed, such as *SpdCas9*-VPR and MS2-MCP-p65-HSF1 or our newly *SpdCas9*-TET1-CD and MS2-MCP-p65-HSF1 combination in transiently transfected Hep3B cells.

It is worth noting that CRISPRa elicited a partial reactivation of the silenced TSGs targeted compared to their physiological gene expression levels in normal hepatocytes. Nonetheless, this approach was still sufficient to elicit significant phenotypic changes in terms of reduced cell proliferation, cell viability, and cell migration, supporting previous work in the context of other TSGs using zinc finger technologies in cancer [18, 72, 73].

For the majority of the TSGs investigated, a single gRNA was sufficient to drive potent re-expression, although at levels that were lower relative to those of normal hepatocytes. For a small number of TSGs (*HHIP* and *CDKN2A*) in HuH-7 cells, a mix of four or five gRNAs was required to elicit significant gene reactivation. This is also consistent with other studies where tiling the gene promoter led to a higher transcriptional reactivation than that achieved by a single gRNA [74, 75]. Consistent with other reports, our data show that the CRISPRa-gRNA design as well as the specific repertoire of epigenetic modifiers that maximize the gene activation state depends on the chromatin context, the targeted gene, and it is, therefore, cell-type specific [68, 76].

In our hands, the synergistic combination of mechanistically distinct effector domains (EDs), such as VPR and MS2-MCP-p65-HSF1, is a powerful tool to endogenously reactivate silenced TSGs in HCC cell lines. These data are consistent with our previous studies in lung and gastric

(See figure on next page.)

Fig. 7 Reactivation of silenced tumor suppressor genes by CRISPRa correlates with phenotypic reprogramming in Hep3B HCC cells. **A, B** Transcriptional reactivation of four silenced tumor suppressor genes (TSGs), *HHIP*, *MT1M*, *PZP*, and *TTC36*, targeted individually and simultaneously (MIX 4 genes) by *SpdCas9*-VPR stably expressed along with the corresponding TSG-gRNA in Hep3B HCC cells. **A** Data shown as fold log10 change in TSG mRNA levels, evaluated by qRT-PCR, relative to *SpdCas9*-VPR with no gRNA (NO G). Data presented as means \pm SEM ($n = 3$) and P values were determined by one-way ANOVA with Dunnett's multiple comparisons test (**** $P < 0.0001$, * $P = 0.0107$). **B** Heatmap comparing the fold change in mRNA regulation evaluated by qRT-PCR. The TSG-gRNAs are arranged in rows, and the genes in columns. Data presented as means ($n = 3$). **C–F** Immunofluorescence of *HHIP*, *MT1M*, *PZP*, *TTC36*, *SpdCas9*-VPR, and Hoechst-stained cell-nuclei in stable Hep3B cells expressing *SpdCas9*-VPR alone (NO G), *SpdCas9*-VPR targeting *HHIP* with G4, *MT1M* with G1, *PZP* with G2, *TTC36* with G3, or *SpdCas9*-VPR co-targeting all four TSGs (MIX 4 genes). **G–I** Phenotypic reprogramming in Hep3B cells lentivirally transduced with *SpdCas9*-VPR targeting and upregulating *HHIP* with G4, *TTC36* with G3, the MIX 4 genes, or with NO G as control. **G** Cell proliferation assessed by α -Ki-67 immunostaining (green), superimposed on nuclear Hoechst 33258 staining (blue). Data normalized to *SpdCas9*-VPR NO G, presented as means \pm SEM ($n = 3$), and P values were determined by unpaired t -test (**** $P < 0.0001$, *** $P = 0.0003$). **H** Cell viability determined using a luminescence assay (CellTiter-Glo®). Data shown as fold change compared to *SpdCas9*-VPR NO G at 24, 48, and 72 h, presented as means \pm SEM ($n = 3$), and P values were determined by unpaired t -test with Welch's correction (**** $P < 0.0001$). **I** Inhibition of cell migration assessed by the Boyden chamber assay. Data normalized to *SpdCas9*-VPR NO G, presented as means \pm SEM ($n = 3$), and P values were determined by unpaired t -test (* $P = 0.0390$, **** $P < 0.0001$, *** $P = 0.0008$)

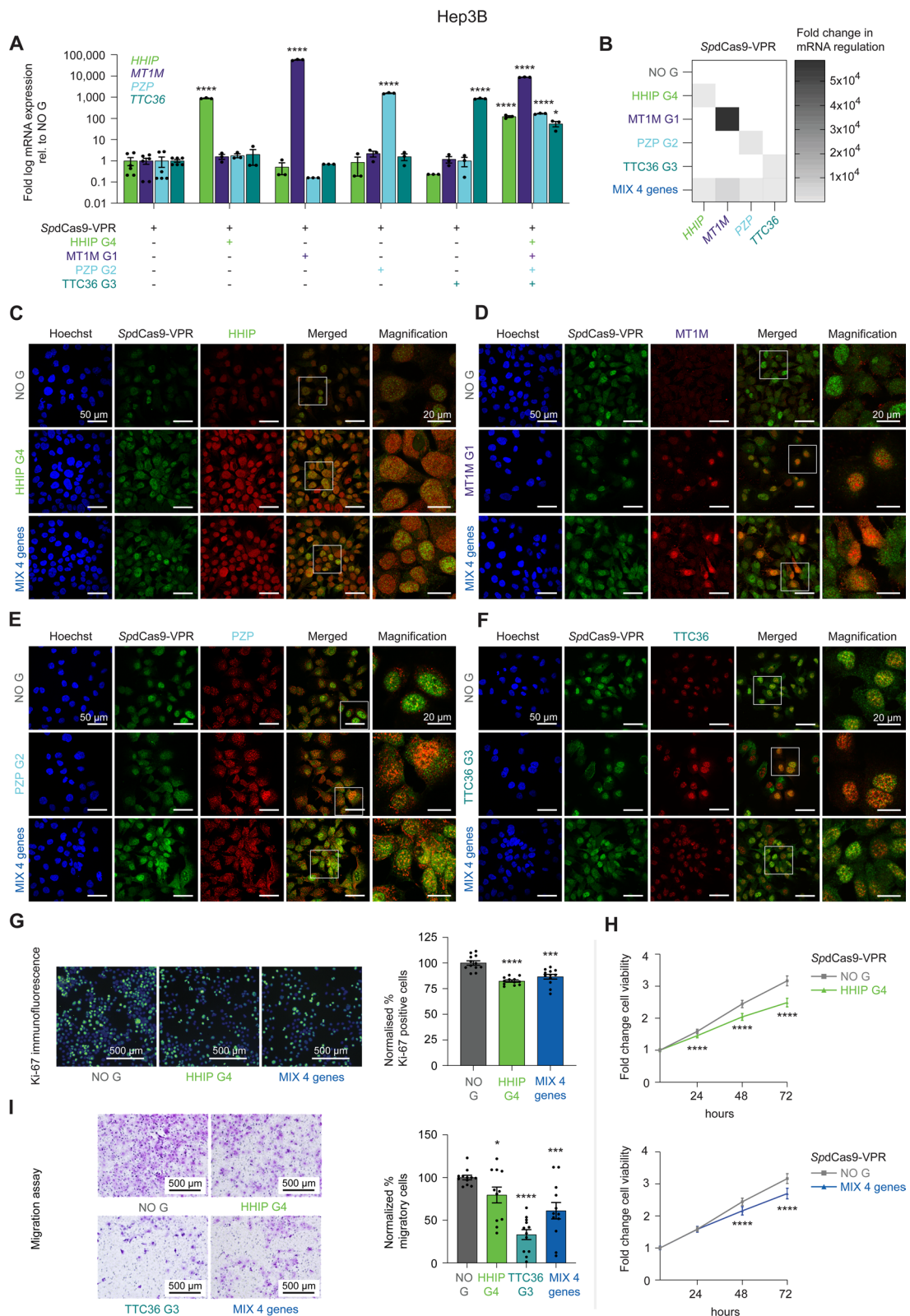


Fig. 7 (See legend on previous page.)

cancer cells both in vitro [18] and in an in vivo breast cancer model [21]. The combination of mechanistically distinct EDs has the potential to recruit a “cloud” of chromatin modifiers that cooperate to catalyze euchromatin formation in the targeted promoter. This suggests that prudent screening of the available epigenetic editing tools might be required for the maximization of the epigenome engineering in HCC.

Importantly, our functional assays indicate that CRISPRa technologies can delineate the role of individual tumor suppressors. This would enable the development of tailored multiplexing strategies to reprogram multiple facets of the HCC phenotype. Among the TSGs tested, we found that CRISPRa-mediated upregulation of *HHIP* decreased HCC proliferation, confirming its role in promoting stemness [43–49] and reinforcing its role as a potential therapeutic target. Moreover, the TSG *TTC36* which is under-expressed in late-stage HCC [62–64], when upregulated by CRISPRa reduced cell migration, demonstrating a potential functional role in controlling cancer cell motility. We also show that CRISPRa-multiplexing of four genes (*HHIP*, *MT1M*, *PZP*, and *TTC36*) could potentially be harnessed to reduce both cell proliferation and migratory potential. Since Hep3B and HuH-7 cells are poorly tumorigenic in mouse models, future studies will require the testing of CRISPRa platforms in additional pre-clinical models, including patient-derived organoids (PDOs) [77] and patient-derived xenografts (PDXs) [78].

Finally, an ongoing challenge for the implementation of epigenetic manipulation in oncology is the targeted delivery of these CRISPRa platforms. One possible strategy is the use of liver-specific AAV8 [79], or the hit-and-run approaches for the delivery of the CRISPRa-encoded biomolecular components, such as in plasmid DNA [21], mRNA [80], or ribonucleoprotein complexes (RNPs) encapsulated in targeted non-toxic cell-released biological nanoparticles [81]. In this context, we recently described synthetic polymeric targeted formulations which can deliver plasmid DNA specifically into human HCC cells [82, 83].

Conclusions

In summary, we have shown that CRISPRa technologies enable the selective activation “at will” of single as well as multiple TSGs silenced in HCC patients. This approach is associated with a significant normalization of the cancer cell phenotype. We have also developed an innovative toolbox that can drive specific and selective epigenetic manipulation of HCC that has the potential to be implemented as a precision oncology approach to treat this highly aggressive cancer.

Methods

Computational analyses

The computational scripts used in this study are available from the associated GitHub repository: https://github.com/jcursons/2022_Sgro_LIHC_tumour_suppressors.

DNA methylation analysis

Illumina Infinium 850K methylation microarray data were imported into R and normalized using the Illumina Human MethylationEPIC Array manifest and missMethyl [84] R/Bioconductor packages. Data were SWAN-normalized [85], and probes were filtered on detection of *P* values before the calculation of *M* and β values. Differential expression analyses were performed on β values using edgeR [86].

Clinical cancer data

Processed RNA-seq, miRNA abundance, and DNAm (probe-level β -value) data from the liver cancer and hepatocellular carcinoma (LIHC) cohort were a subset from The Cancer Genome Atlas (TCGA) Pan-Cancer Clinical Data Resource (TCGA-CDR) [87].

The Cancer Genome Atlas (TCGA) data

Analysis of the TCGA liver cancer data was performed using Python (v 3.7.4) with the SciPy [88], pandas [89], Matplotlib [90], and NumPy [91] libraries. Processed TCGA molecular data were downloaded from <https://gdc.cancer.gov/about-data/publications/pancanatlas> and annotated with patient data from the TCGA-CDR [87] and the original TCGA-LIHC manuscript [12].

Integrated-data cluster (iClust) inference

The original TCGA-LIHC manuscript [12] used an integrated data set with DNA copy number, gene methylation, miRNA abundance, and RNA abundance and performed clustering to identify 3 ‘iClusters’. A number of samples were excluded from this classification as they did not have data available across all of the associated platforms. To infer the iCluster values of unspecified samples for further analysis in this study, a differential gene expression analysis was performed between samples of known iClust values using limma and edgeR. Differentially expressed gene lists were used as signatures for gene set scoring with the *singscore* package [92], and scores for the three iClust gene sets were used for a *k*-nearest neighbors classification ($n_{\text{neighbors}} = 30$) with the scikit-learn [93] package. Samples were assigned to the iClust with the highest probability predicted by this classifier (Additional file 1: Fig. S1).

RNA-seq and methylation data from the Cancer Cell Line Encyclopedia (CCLE)

We downloaded the RNA-seq count data (Feb 2020) and methylation data (Aug 2020) of liver cancer cell lines from the Cancer Cell Line Encyclopedia (CCLE) (<https://data.broadinstitute.org/ccle/>) and used R version 4.0.5 to compare the two data types. For the RNA-seq data, we retained genes with a count > 5 in at least five cell lines, performed TMM normalization [94], calculated log RPKM values using the `rpkm` function in the `edgeR` package (v 3.32.1) [86], and used the gene length information from GENCODE version 19. The `tidyr` (v 1.1.3, including `ggplot2`) package was used for data manipulation and visualization.

Cell culture

Hep3B and HuH-7 HCC cell lines (a gift from Professor Peter J. Leedman's Laboratory) were cultured in DMEM low glucose-pyruvate supplemented containing 10% HyClone fetal bovine serum (FBS) (GE Healthcare Life Sciences, Cat. No. SH30084.03) and 1% antibiotic-antimycotic (Gibco, Cat. No. 15240062). HEK293T cells (ATCC, Cat. No. CRL-3216) were grown in DMEM high glucose-pyruvate containing 10% FBS and 1% antibiotic-antimycotic. The immortalized human liver cell line THLE-3 (ATCC, Cat. No. CRL-1123) was grown in BEBM supplemented with BEGM Bullet Kit (Lonza, Cat. No. CC-3170), from which we omitted the gentamycin/amphotericin and epinephrine, and to which we added 5 ng/mL human epidermal growth factor (EGF) recombinant protein (Gibco, Cat. No. PHG0311), 70 ng/mL *O*-Phosphorylethanolamine (Sigma-Aldrich, Cat. No. P0503), and 10% FBS. These cells were maintained in flasks pre-coated with a mixture of 0.01 mg/mL human fibronectin (Gibco, Cat. No. 33016015), 0.03 mg/mL bovine collagen type I (Australian Biosearch, Cat. No. 5005-B), and 0.01 mg/mL bovine serum albumin (Sigma-Aldrich, Cat. No. A9647) dissolved in BEBM medium (Lonza). All cell lines used in this study were *Mycoplasma*-free and maintained at 37 °C and 5% CO₂.

Normal hepatocytes

Total RNA from a donor's healthy normal liver was extracted using the RNeasy Plus Mini Kit (Qiagen, Cat. No. 74134) as per the manufacturer's instructions, under the conditions of the ethical approval (RGS0000001834) granted to Professor George C.T. Yeoh by the Human Research Ethics Committee at the Sir Charles Gairdner Hospital, Perth, Western Australia.

Drug treatments

Hep3B and HuH-7 cells were seeded in complete medium in 6-well plates at a concentration of 6×10^4 for treatments with 5-aza-2'-deoxycytidine, i.e., decitabine (Selleckchem, Cat. No. S1200, Batch No.09) or 15×10^4 for treatments with suberoylanilide hydroxamic acid (SAHA), i.e., vorinostat (Selleckchem, Cat. No. S1047, Batch No.11). Twenty-four hours later, the cells were treated with 5-aza-2'-deoxycytidine or SAHA at concentrations of 1, 2.5, 5, 7.5, and 10 μ M or 1, 2, and 4 μ M for 72 or 48 h, respectively. The culture medium was replaced daily, and dimethyl sulfoxide (DMSO) was used as vehicle control. Cells were subsequently collected for RNA extraction.

gRNA designing and off-target identification

Four to five candidate gRNA sequences for gene activation, with optimized on- and off-target scores [33, 34] (<https://benchling.com/>), were selected within the proximal promoter and CpG islands of each targeted TSG (Additional file 10: Table S1). To search for potential genomic off-target binding sites with three mismatches or less to the cognate most active TSG-targeting gRNA sequences, the algorithm Cas-OFFinder [35] was implemented. The genomic location for each off-target sequence was bioinformatically mapped on the UCSC Genome Browser with the integrated information relevant to the regulation of transcription from the ENCODE project. The off-target sequences found in proximity to gene regulatory elements were assessed by qRT-PCR in transiently transfected and lentivirally transduced cells (Additional file 4, 5: Fig. S4 and Additional file 16: Data S5).

Plasmids

The plasmids utilized for transient transfections in this study were pcDNATM3.1 (+) empty vector Zeo backbone (Invitrogen, Cat. No. V790-20); pUC19 sgRNA cloning backbone with MS2 loops at tetraloop and stem-loop 2 that contains BbsI sites for insertion of spacer sequences (Addgene plasmid # 61424, a gift from Feng Zhang); MS2-p65-HSF1_GFP (Addgene plasmid # 61423, a gift from Feng Zhang); SP-dCas9-VPR (Addgene plasmid # 63798, a gift from George Church); pdCas9-Tet1-CD and pcDNA3.1-MS2-Tet1-CD (Addgene plasmids # 83340 and # 83341, respectively, a gift from Ronggui Hu); and pcDNA-dCas9 (Addgene plasmid # 47106, a gift from Charles Gersbach).

The plasmids utilized for lentiviral transductions in this study were pMD2.G (VSV-G envelope expressing

plasmid) and the third generation packaging pMDLg/pRRE (GAG and POL expressing plasmid) (Addgene plasmids # 12259 and # 12251, respectively, a gift from Didier Trono), pLV hU6-sgRNA hUbc-dCas9-VPR-T2A-Puro [19], and pLV hU6-sgRNA hUbc-dCas9-TET1-CD-T2A-Puro (this paper, see Molecular cloning section).

Molecular cloning

The pLV hU6-sgRNA hUbc-dCas9-TET1-CD-T2A-Puro lentiviral vector was generated from the pLV hU6-sgRNA hUbc-dCas9-KRAB-T2A-Puro (Addgene plasmid # 71236, a gift from Charles Gersbach) by replacing the KRAB domain with the catalytic domain of TET-1 from Fuw-dCas9-Tet1CD (Addgene plasmid # 84475, a gift from Rudolf Jaenisch).

For each gRNA, sense and anti-sense customized DNA oligonucleotides (IDT, Integrated DNA Technologies) were annealed and ligated, using T4 DNA ligase (Promega, Cat. No. M1801), into the BbsI recognition site of the transient pUC19 sgRNA (MS2) cloning backbone or into the BsmBI recognition site of the lentiviral vectors pLV hU6-sgRNA hUbc-dCas9-VPR-T2A-Puro and pLV hU6-sgRNA hUbc-dCas9-TET1-CD-T2A-Puro.

Transient transfection

Hep3B and HuH-7 cells were seeded in a complete culture medium at a density of 3.5×10^5 cells/well in 6-well plates 18 h prior to transfection using Lipofectamine 3000 (Invitrogen, Cat. No. L3000001). The next day, the cells were incubated with a transfection mix containing transfection reagents and 2.55 μ g of plasmid DNA in Opti-MEM (Gibco), according to the manufacturer's protocol. The culture medium containing the transfection mix was removed after 4 h and exchanged for fresh culture medium. Cells were collected 48 h post-transfection to assess mRNA upregulation of VPR/gRNA-MS2-MCP-p65-HSF1 activator constructs based on our previous work [18]. Cells were also harvested 72 h post-transfection to determine mRNA modulation when tiling the proximal promoter with TET1-CD systems, and 96 h post-transfection for RNA extraction and DNA methylation assays to provide additional cell division cycles for DNA demethylation activities when employing TET1-CD-based constructs, as previously described [67].

Quantitative real-time PCR (qRT-PCR)

Total RNA was extracted from cultured, transfected, and transduced cells using QIAzol Lysis Reagent (Qiagen) as per the manufacturer's protocol. 1000 ng of extracted RNA was used for cDNA synthesis using a High-Capacity cDNA Reverse Transcription Kit or a TaqMan[™] MicroRNA Reverse Transcription Kit (Applied Biosystems). Relative quantification of the transcript expression was

obtained by qRT-PCR using TaqMan probes in a ViiA[™] 7 Real-Time PCR System (Applied Biosystems). The TaqMan probes utilized are listed in Additional file 11: Table S2. The data were analyzed using the $\Delta\Delta C_t$ method [95] with *GAPDH*, *GUSB*, *PPIA*, and *RNU6B* as house-keeping genes for normalization.

Genomic DNA purification

Genomic DNA was obtained from Hep3B cells seeded at a density of 3.5×10^5 cells/well in 6-well plates and transiently transfected for 96 h. Cells were washed in Dulbecco's PBS (DPBS), collected, and centrifuged at 1000 rpm for 5 min at room temperature. Pelleted cells were washed in DPBS and centrifuged again. Cell pellets were then processed using a Monarch[®] Genomic DNA Purification Kit (NEB, Cat. No. T3010L) according to the manufacturer's protocol. Genomic DNA was shipped at room temperature to the AGRF (Australian Genome Research Facility, Melbourne) for DNA methylation analysis using an Illumina Infinium 850K methylation microarray. Bisulfite-converted DNA was amplified, fragmented, and hybridized to Illumina Infinium MethylationEPIC Bead-Chip Kit using standard Illumina protocol.

Lentiviral production and transduction

Hep3B cells were transduced with lentivirus to constitutively co-express *SpdCas9-VPR* [19] or *SpdCas9-TET1-CD* (this paper) along with the tumor suppressor gene (TSG)-targeting gRNAs (CRISPRa). Lentiviral particles were generated by transfecting HEK293T cells with 4.5 μ g of CRISPRa lentiviral expression plasmid, 1.54 μ g of pMD2.G (VSV-G envelope expressing plasmid), and 2.88 μ g of pMDLg/pRRE (GAG and POL expressing plasmid) mixed with 50 μ L of Lipofectamine 2000 (Thermo Fisher Scientific, Cat. No. 11668019) in Opti-MEM (Gibco). After 4 h, the transfection medium was replaced with HEK293T medium. The supernatants containing lentivirus were collected for transduction 42, 50, and 66 h after the first medium exchange, and cleared from residual producer cells by filtration through 0.22 μ m hydrophilic PVDF membrane syringe filters (Millipore). The cationic polymer polybrene (Sigma-Aldrich, Cat. No. 107689) was added to the filtered viral supernatants at a concentration of 8 μ g/mL to promote transduction. Hep3B cells, plated in 10 cm plates, were transduced three times with the lentiviral particles, for a period of 8–12 h each time. For the combination of gRNAs (MIX 4G) or for genome multiplexing (MIX 4 genes), equal volumes of lentiviral particles were added to the host cells. Eight hours after the last transduction, the medium was replaced with a fresh medium to remove the virus. Transduced cells with lentivirus containing a puromycin-resistance gene were treated with 1.75 μ g/mL puromycin

(Gibco, Cat. No. A1113803) 72 h after transduction to initiate selection.

Immunofluorescence

Hep3B cells lentivirally transduced with *SpdCas9-VPR* (CRISPRa) were seeded at a density of 2.5×10^4 cells onto 13-mm glass coverslips pre-treated with poly-L-lysine hydrobromide (Sigma-Aldrich, Cat. No. P6282). Twenty-four hours after seeding, the adhered cells were fixed with 4% Pierce™ Formaldehyde Methanol-free (Thermo Fisher Scientific, Cat. No. 28908) in DPBS for 20 min at room temperature and washed twice with DPBS. Fixed cells were blocked with 5% normal goat serum (Invitrogen, Cat. No. 31872) and 0.3% Triton X-100 (Sigma-Aldrich) in DPBS for 1 h at room temperature, then incubated with α -Ki-67 mouse monoclonal antibody (Cell Signaling Technology, Cat. No. 9449, 1:500) in diluent buffer (1% BSA and 0.3% Triton X-100 in DPBS) overnight at 4 °C. The next day, the cells were washed and incubated with a goat α -mouse secondary Alexa Fluor 488-conjugated antibody (Thermo Fisher Scientific, Cat. No. A11001, 1:500) for 2 h at room temperature. The coverslips were mounted on slides with SlowFade™ Diamond Antifade Mountant (Thermo Fisher Scientific, Cat. No. S36963) and the percentage of cells positive for Ki-67 versus the total number of cells counterstained with Hoechst 33258 (Sigma-Aldrich, Cat. No. 94403, 1:5,000) was assessed in 12 fields of view from images acquired with an Olympus DP71 fluorescence microscope.

For protein detection of the four genes targeted by *SpdCas9-VPR* (CRISPRa), the primary antibodies used were α -HHIP rabbit polyclonal (Invitrogen, Cat. No. PA5-22242, 1:400), α -MT1M rabbit polyclonal (ProteinTech, Cat. No. 17281-1-AP, 1:200), α -PZP rabbit polyclonal (Abcam, Cat. No. ab233166, 1:20), α -TTC36 rabbit polyclonal (Abcam, Cat. No. ab122507, 1:300), and α -*SpCas9* mouse monoclonal [7A9-3A3] (Abcam, Cat. No. ab191468, 1:500). The secondary antibodies used were Alexa Fluor 488-conjugated goat α -mouse (Thermo Fisher Scientific, Cat. No. A11001, 1:500) and Alexa Fluor 594-conjugated goat α -rabbit (Thermo Fisher Scientific, Cat. No. A11012, 1:500); Hoechst 33258 was used to stain the cell nuclei. Images were acquired by a confocal fluorescence Nikon Ti-E inverted microscope using a Nikon Plan Apo VC 60x/1.40 Oil OFN25 DIC N2 objective and collected using NIS-C Elements Software.

Cell viability assay

Hep3B cells lentivirally transduced with CRISPRa were seeded at a density of 5×10^3 cells/well in complete medium in 96-well white-bottom plates (Greiner) and processed after 4, 24, 48, and 72 h with CellTiter-Glo® 2.0 (Promega, Cat. No. G9241) luminescence assay protocol

to determine cell viability. The luminescence was measured using a CLARIOstar plate reader (BMG Labtech, Mornington, VIC, Australia). The luciferase measurements were normalized to CRISPRa NO G control.

Migration assay

Hep3B cells lentivirally transduced with CRISPRa were seeded at the concentration of 5×10^4 in serum-free medium in the inner chamber of Costar® Transwell cell culture inserts (6.5 mm diameter, 8 μ m pore size, Corning, Cat. No. 3422). A complete medium containing 10% FBS was added to the outer chamber as a chemoattractant, and the cells were incubated for 48 h. The inserts were stained as per protocol using a staining solution containing 0.5% crystal violet dissolved in 25% methanol and sterile water for 10 min. Images from 12 fields of view were acquired with an inverted Leica light microscope to quantify the percentage of cells that had migrated, based on biological triplicates, using ImageJ software.

Statistical analyses

All data were derived from multiple experiments conducted at least in triplicate. Statistical analyses were performed with Prism 9 (GraphPad Software, La Jolla, CA, USA) and are detailed in the figure legends. For iCluster signature derivation, differential gene expression was performed in R (v 3.6.1; <https://www.r-project.org/>) using limma [96] with a Benjamini–Hochberg correction and TREAT criteria ($\log_{FC} > 1.5$, adj. P value < 0.05) [97]. The identification of differentially methylated probes was performed using limma with a Benjamini–Hochberg correction.

Supplementary Information

The online version contains supplementary material available at <https://doi.org/10.1186/s13148-023-01482-0>.

Additional file 1: Figure S1. Related to Fig. 1. A Scatter plots showing the associations between different integrated-data cluster (iClust) scores of individual tumor samples. Tumor samples with an iClust value specified in the original TCGA manuscript are shown (*dark blue, dark orange, and dark green*), together with inferred iClust annotations (*light blue, light orange, and light green*) obtained through a k-nearest neighbors' classification (further details given in "Methods").

Additional file 2: Figure S2. Related to Fig. 1. A The percentage of patients who have evidence of gene hypermethylation and no evidence of gene loss/deletion within each iCluster group (iClust1: *blue*; iClust2: *orange*; and iClust3: *green*) and across all patients (*black*). **B** The percentage of patients who have evidence of gene hypermethylation and no evidence of gene loss/deletion in at least one gene of the listed set, within each iCluster group and across all patients. Genes were defined as hypermethylated if their corresponding probe β -value was greater than all matched-adjacent/normal liver tissue samples

Additional file 3: Figure S3. Related to Fig. 2. A Anticorrelation between RNA abundance (from RNA-seq data) and DNA methylation data of the available genes (*CPS1, HHIP, MT1E, MT1M, PSAT1, PTGR1, TMEM106A,*

and *TTC36*) for Hep3B and HuH-7 HCC cell lines from the Cancer Cell Line Encyclopedia. RPKM, Reads Per Kilobase Million.

Additional file 4: Figure S4 (part 1). Related to Figs. 3–7. A Off-target analysis of the ten TSGs reactivated in this study, using the most potent gRNAs. The potential off-target genes (*MMP11*, *MOCOS*, *PIR*, *SEMA5A*, *TMEM14C*, *HRH1*, *NACC2*, *NONO*, *PPA1*, *RBM39*, *NKAIN3*, and *ABCC3*) were found in proximity to genomic regulatory regions.

Additional file 5: Figure S4 (part 2). Related to Figs. 3–7. CRISPRa is highly specific in hit-and-run and lentiviral approaches in HCC cell lines. A–K The potential off-target genes (*MMP11*, *MOCOS*, *PIR*, *SEMA5A*, *TMEM14C*, *HRH1*, *NACC2*, *NONO*, *PPA1*, *RBM39*, *NKAIN3*, and *ABCC3*) found in proximity to genomic regulatory regions for the most potent gRNAs utilized were assessed by qRT-PCR 48 h post-transfection, employing *SpdCas9*-VPR and MS2-MCP-p65-HSF1 system in HuH-7 (A), (B), (C), (E) and Hep3B cells (F), (H), (J); and in stable Hep3B cell lines expressing *SpdCas9*-VPR (D), (G), (I), (K). Relative gene expression, expressed as fold change, was normalized to cells transfected with empty vector control (EV) or to cells transfected with *SpdCas9*-VPR NO G, and compared to either EV or NO G conditions for statistical analysis. Data presented as means \pm SEM ($n = 3$), and P -values were determined by two-way ANOVA with Dunnett's multiple comparisons test for panels (A), (B), (C), (E), (F), (H), and (J) (A: $***P = 0.0001$; B, C, E, F, and H: $****P < 0.0001$; J: $***P = 0.0003$, $****P < 0.0001$); or by two-way ANOVA with Šidák's multiple comparisons test for panels D, G, I, and K ($****P < 0.0001$).

Additional file 6: Figure S5. Related to Fig. 5. Tiling the promoter of MT1M and TTC36 tumor suppressor genes with a CRISPRa toolbox in Hep3B HCC cells. A–B Fold change in *MT1M* (A) and *TTC36* (B) mRNA expression evaluated by qRT-PCR 72 h after transient transfection in Hep3B cells. Cells were transfected with combinations of CRISPRa along with a mix of four gRNAs (MIX 4G), or with no gRNA (NO G) as control. Relative gene expression was normalized and compared to cells transfected with empty vector control (EV) for statistical analysis. Data presented as means \pm SEM ($n = 3$), and P -values were determined by one-ANOVA with Dunnett's multiple comparisons test ($****P < 0.0001$). *SpdCas9 Streptococcus pyogenes* deactivated Cas9 protein adopted for epigenome engineering, VPR VP64, p65, Rta, MS2 RNA aptamer, MCP MS2-coat protein, HSF1 heat shock factor 1, TET1-CD Ten-Eleven Translocation methylcytosine dioxygenase 1-catalytic domain, MIX 4G combination of four gRNAs.

Additional file 7: Figure S6. Related to Fig. 5. Transcriptional reactivation of HHIP gene by novel CRISPRa combinations does not correlate with changes in promoter DNA methylation in transiently transfected Hep3B cells. A Fold change in *HHIP* mRNA expression evaluated by qRT-PCR 96 h after transient transfection in Hep3B cells. Cells were transfected with *SpdCas9*-VPR and MS2-MCP-p65-HSF1, or with *SpdCas9*-TET1-CD and MS2-MCP-p65-HSF1, along with gRNA G4 or with no gRNA (NO G) as control. Relative gene expression was normalized and compared to cells transfected with empty vector control (EV) for statistical analysis. Data presented as means \pm SEM ($n = 3$), and P -values were determined by unpaired t -test ($***P = 0.0001$, $****P < 0.0001$). **B** Heatmap showing *HHIP* promoter DNA methylation in Hep3B cells transiently transfected with the novel CRISPRa combinations. Data from Illumina Infinium 850 K methylation EPIC microarrays. For each probe (listed at left), the difference in β -value from the average is shown (at left; green-purple color map) together with the average probe β -value (at center; blue-yellow color map), and the adjusted P -value for differential methylation between gRNA G4 and NO G for the two combinations tested (at right; white-purple color map).

Additional file 8: Figure S7. Related to Fig. 5. Lentiviral transduction of SpdCas9-TET1-CD or SpdCas9-VPR targeting HHIP or MT1M genes in Hep3B cells. A Schematic representation of the "all-in-one" lentiviral vectors, *SpdCas9*-TET1-CD and *SpdCas9*-VPR, for the constitutive co-expression of a gRNA and TET1-CD or VPR, C-terminally fused to *SpdCas9*. **B** Fold change in *HHIP* mRNA expression assessed by qRT-PCR at 18, 30, and 40 days in Hep3B cells constitutively co-expressing *SpdCas9*-TET1-CD and the combination of four gRNAs (MIX 4G) targeting *HHIP* promoter. **C** Fold change in *MT1M* mRNA expression assessed by qRT-PCR at 20 days in Hep3B cells lentivirally co-transduced with *SpdCas9*-TET1-CD and

individual gRNAs (G1, G2, G3, and G4) or the MIX 4G; or with *SpdCas9*-VPR and the most potent gRNA (G1). Data presented as means \pm SEM ($n = 3$), compared to *SpdCas9*-TET1-CD NO G, and P -values were determined by two-way ANOVA with Šidák's multiple comparisons test for panel (B), and by two-way ANOVA with Dunnett's multiple comparisons test for panel (C) ($****P < 0.0001$). *SpdCas9 Streptococcus pyogenes* deactivated Cas9 protein adopted for epigenome engineering, TET1-CD Ten-Eleven Translocation methylcytosine dioxygenase 1-catalytic domain, VPR VP64, p65, Rta, hU6 RNA polymerase III promoter for human U6 snRNA, hUbc human ubiquitin C promoter, 3xFLAG three tandem FLAG[®] epitope tags, followed by an enterokinase cleavage site, SV40NLS nuclear localization signal of SV40 (simian virus 40) large T antigen, T2A 2A peptide from *Thoesa asigna* virus capsid protein, cleavable linker, PuroR puromycin N -acetyltransferase gene that confers resistance to puromycin, MIX 4G combination of four gRNAs, ns not significant.

Additional file 9: Figure S8. Related to Fig. 7. Phenotypic reprogramming in Hep3B HCC cells lentivirally transduced with SpdCas9-VPR targeting and upregulating MT1M with G1, PZP with G2, TTC36 with G3, or with NO G as control. A–C Cell viability determined using a luminescence assay (CellTiter-Glo[®]). Data shown as fold change compared to *SpdCas9*-VPR NO G at 24, 48, and 72 h, presented as means \pm SEM ($n = 3$), and P -values were determined by unpaired t -test with Welch's correction (From left to right: (A), $***P = 0.0001$, $**P = 0.0056$; (B), $**P = 0.0024$, $*P = 0.0011$; and (C), $****P < 0.0001$, $*P = 0.0310$). **D** Cell migration assessed by the Boyden chamber assay. Data normalized to *SpdCas9*-VPR NO G, presented as means \pm SEM ($n = 3$), and P -values were determined by unpaired t -test. ns not significant.

Additional file 10: Table S1. Related to Figs. 3–7 and Figures S4–S8. gRNAs designed for gene reactivation by CRISPRa technology. Details include gRNA and PAM sequences, the DNA strand targeted, the distance from the TSS, and the genomic annotations.

Additional file 11: Table S2. Related to Figs. 2–7 and Figures S4–S7. TaqMan gene expression assays utilized for qRT-PCR experiments.

Additional file 12: Data S1. Related to Fig. 1. Assigned 'integrated cluster' (iClust) groups for TCGA liver cancer samples where available (from the original TCGA-LHC manuscript), together with inferred iClusters for unspecified samples, as determined by clustering of gene set scores (as shown in Figure S1; further details given in "Methods").

Additional file 13: Data S2. Related to Fig. 1. mRNA transcript abundance, probe methylation (beta) values, and copy number variation data for all TCGA liver samples (including matched adjacent normal liver tissue). Corresponds to pre-transformed data shown in Fig. 1.

Additional file 14: Data S3. Related to Fig. 1. z-score normalized mRNA transcript abundance, probe methylation (beta) values, and copy number variation for all TCGA liver samples (including matched adjacent normal liver tissue). Corresponds to data shown in Fig. 1.

Additional file 15: Data S4. Related to Fig. 2, Fig. 3, Fig. 4, and Fig. 6. Comparison of the fold change in mRNA expression for the tumor suppressor genes targeted individually or multiplexed by CRISPRa system (*SpdCas9*-VPR and MS2-MCP-p65-HSF1) versus treatments with the epidugs (5-aza and SAHA) in Hep3B and HuH-7 cells.

Additional file 16: Data S5. Related to Figs. 3, 4, and 7. Comprehensive bioinformatic analysis of predicted potential off-targets for the ten TSGs targeted by CRISPRa technology utilizing the most active gRNAs.

Additional file 17: Data S6. Related to Figure S6. Probe methylation (beta) values for *HHIP* in transiently transfected Hep3B cells with *SpdCas9*-VPR and MS2-MCP-p65-HSF1, or *SpdCas9*-TET1-CD and MS2-MCP-p65-HSF1 targeting *HHIP* promoter.

Acknowledgements

The authors thank Dr. Robin Scaife (The Harry Perkins Institute of Medical Research) for critical reading and editing of the manuscript, Clinical Associate Professor Lingjun Mou (WA Liver and Kidney Surgical Transplant Service at Sir Charles Gairdner Hospital) for providing the normal liver sample, and Professor

Leandro Sgro (The Istituto Europeo di Design, IED) for his assistance in generating schematic figures depicting the CRISPRa technology.

Author contributions

AS contributed to the investigation, study design, execution of the experiments, data analysis and interpretation, off-target analysis, figure construction, and wrote the manuscript. JC, GCTY, and PB contributed to the study inception. CW contributed to the gRNA design. JC, MF, and RL contributed to the bioinformatic data analysis. EAW contributed to the confocal microscopy imaging. PJL and GCTY contributed to the revision of the manuscript. PB contributed to the conceptualization, supervision, and edited the manuscript. All authors read and approved the final manuscript.

Funding

This study was funded by the following grants awarded to PB: the Australian Research Council (ARC) Future Fellowship FT130101767, the Cancer Council of Western Australia (CCWA) Research Fellowship program, and the National Health and Medical Research Council (NHMRC) Grant APP1165208 (recipients: PB, JC, and GCTY). AS was supported by an Australian Government Research Training Program (RTP) Ph.D. Scholarship.

Availability of data and materials

All data generated or analyzed during this study are included in this article. DNAm data generated in this study are available from the Gene Expression Omnibus page (<https://www.ncbi.nlm.nih.gov/geo/>) under accession number GSE211837. Patient data were downloaded from The Cancer Genome Atlas (<https://gdc.cancer.gov/about-data/publications/pancanatlas>) and Cancer Cell Line Encyclopedia (CCLE) data were downloaded from the Cancer Dependency Map (<https://depmap.org/portal/download/>).

Declarations

Ethics approval and consent to participate

Not applicable.

Consent for publication

Not applicable.

Competing interests

The authors declare no conflict of interest.

Received: 22 November 2022 Accepted: 9 April 2023

Published online: 29 April 2023

References

- Rumgay H, Ferlay J, de Martel C, Georges D, Ibrahim AS, Zheng R, et al. Global, regional and national burden of primary liver cancer by subtype. *Eur J Cancer*. 2022;161:108–18.
- Tarao K, Nozaki A, Ikeda T, Sato A, Komatsu H, Komatsu T, et al. Real impact of liver cirrhosis on the development of hepatocellular carcinoma in various liver diseases-meta-analytic assessment. *Cancer Med*. 2019;8(3):1054–65.
- Schulze K, Nault JC, Villanueva A. Genetic profiling of hepatocellular carcinoma using next-generation sequencing. *J Hepatol*. 2016;65(5):1031–42.
- Toh TB, Lim JJ, Chow EK. Epigenetics of hepatocellular carcinoma. *Clin Transl Med*. 2019;8(1):13.
- Llovet JM, Kelley RK, Villanueva A, Singal AG, Pikarsky E, Roayaie S, et al. Hepatocellular carcinoma. *Nat Rev Dis Primers*. 2021;7(1):6.
- Roayaie S, Obeidat K, Sposito C, Mariani L, Bhoori S, Pellegrinelli A, et al. Resection of hepatocellular cancer ≤ 2 cm: results from two Western centers. *Hepatology*. 2013;57(4):1426–35.
- Rinaldi L, Vetrano E, Rinaldi B, Galiero R, Caturano A, Salvatore T, et al. HCC and molecular targeting therapies: back to the future. *Biomedicines*. 2021;9(10):1345.
- Zhu YJ, Zheng B, Wang HY, Chen L. New knowledge of the mechanisms of sorafenib resistance in liver cancer. *Acta Pharmacol Sin*. 2017;38(5):614–22.
- Sangro B, Chan SL, Meyer T, Reig M, El-Khoueiry A, Galle PR. Diagnosis and management of toxicities of immune checkpoint inhibitors in hepatocellular carcinoma. *J Hepatol*. 2020;72(2):320–41.
- Xu X, Jiang W, Han P, Zhang J, Tong L, Sun X. MicroRNA-128-3p mediates Lenvatinib resistance of hepatocellular carcinoma cells by downregulating c-Met. *J Hepatocell Carcinoma*. 2022;9:113–26.
- Shi W, Zhang S, Ma D, Yan D, Zhang G, Cao Y, et al. Targeting SphK2 reverses acquired resistance of regorafenib in hepatocellular carcinoma. *Front Oncol*. 2020;10:694.
- Cancer Genome Atlas Research Network. Electronic address wbe, Cancer Genome Atlas Research N. Comprehensive and integrative genomic characterization of hepatocellular carcinoma. *Cell*. 2017;169(7):1327–41 e23.
- Csepregi A, Ebert MP, Rocken C, Schneider-Stock R, Hoffmann J, Schulz HU, et al. Promoter methylation of CDKN2A and lack of p16 expression characterize patients with hepatocellular carcinoma. *BMC Cancer*. 2010;10:317.
- Zhou Y, Wang XB, Qiu XP, Shuai Z, Wang C, Zheng F. CDKN2A promoter methylation and hepatocellular carcinoma risk: a meta-analysis. *Clin Res Hepatol Gastroenterol*. 2018;42(6):529–41.
- Esteller M. Epigenetics in cancer. *N Engl J Med*. 2008;358(11):1148–59.
- Xiao W, Zhou Q, Wen X, Wang R, Liu R, Wang T, et al. Small-molecule inhibitors overcome epigenetic reprogramming for cancer therapy. *Front Pharmacol*. 2021;12:702360.
- Lu Y, Chan YT, Tan HY, Li S, Wang N, Feng Y. Epigenetic regulation in human cancer: the potential role of epi-drug in cancer therapy. *Mol Cancer*. 2020;19(1):79.
- Garcia-Bloj B, Moses C, Sgro A, Plani-Lam J, Arooj M, Duffy C, et al. Waking up dormant tumor suppressor genes with zinc fingers, TALEs and the CRISPR/dCas9 system. *Oncotarget*. 2016;7(37):60535–54.
- Moses C, Nugent F, Waryah CB, Garcia-Bloj B, Harvey AR, Blancafort P. Activating PTEN tumor suppressor expression with the CRISPR/dCas9 system. *Mol Ther Nucleic Acids*. 2019;14:287–300.
- Kardooni H, Gonzalez-Gualda E, Stylianakis E, Saffaran S, Waxman J, Kypta RM. CRISPR-mediated reactivation of DKK3 expression attenuates TGF-beta signaling in prostate cancer. *Cancers (Basel)*. 2018;10(6):165.
- Kretzmann JA, Evans CW, Moses C, Sorolla A, Kretzmann AL, Wang E, et al. Tumour suppression by targeted intravenous non-viral CRISPRa using dendritic polymers. *Chem Sci*. 2019;10(33):7718–27.
- Zhou X, Li R, Jing R, Zuo B, Zheng Q. Genome-wide CRISPR knockout screens identify ADAMTSL3 and PTEN genes as suppressors of HCC proliferation and metastasis, respectively. *J Cancer Res Clin Oncol*. 2020;146(6):1509–21.
- Wei L, Lee D, Law CT, Zhang MS, Shen J, Chin DW, et al. Genome-wide CRISPR/Cas9 library screening identified PHGDH as a critical driver for Sorafenib resistance in HCC. *Nat Commun*. 2019;10(1):4681.
- Cai J, Chen J, Wu T, Cheng Z, Tian Y, Pu C, et al. Genome-scale CRISPR activation screening identifies a role of LRP8 in Sorafenib resistance in hepatocellular carcinoma. *Biochem Biophys Res Commun*. 2020;526(4):1170–6.
- Freese K, Seitz T, Dietrich P, Lee SML, Thasler WE, Bosserhoff A, et al. Histone deacetylase expressions in hepatocellular carcinoma and functional effects of histone deacetylase inhibitors on liver cancer cells in vitro. *Cancers (Basel)*. 2019;11(10):1587.
- Lai MJ, Huang HL, Pan SL, Liu YM, Peng CY, Lee HY, et al. Synthesis and biological evaluation of 1-arylsulfonyl-5-(N-hydroxyacrylamide)indoles as potent histone deacetylase inhibitors with antitumor activity in vivo. *J Med Chem*. 2012;55(8):3777–91.
- Gailhouste L, Liew LC, Yasukawa K, Hatada I, Tanaka Y, Nakagama H, et al. Differentiation therapy by epigenetic reconditioning exerts antitumor effects on liver cancer cells. *Mol Ther*. 2018;26(7):1840–54.
- Sajadian SO, Tripura C, Samani FS, Ruoss M, Dooley S, Baharvand H, et al. Vitamin C enhances epigenetic modifications induced by 5-azacytidine and cell cycle arrest in the hepatocellular carcinoma cell lines HLE and Huh7. *Clin Epigenet*. 2016;8:46.
- Sanaei M, Kavooosi F. Effect of vorinostat on INK4 family and HDACs 1, 2, and 3 in pancreatic cancer and hepatocellular carcinoma. *Res Pharm Sci*. 2021;16(3):260–8.
- Kim DY, Cheong HT, Ra CS, Kimura K, Jung BD. Effect of 5-azacytidine (5-aza) on UCP2 expression in human liver and colon cancer cells. *Int J Med Sci*. 2021;18(10):2176–86.

31. Chavez A, Scheiman J, Vora S, Pruitt BW, Tuttle M, Iyer EPR, et al. Highly efficient Cas9-mediated transcriptional programming. *Nat Methods*. 2015;12(4):326–8.
32. Konermann S, Brigham MD, Trevino AE, Joung J, Abudayyeh OO, Barcena C, et al. Genome-scale transcriptional activation by an engineered CRISPR-Cas9 complex. *Nature*. 2015;517(7536):583–8.
33. Hsu PD, Scott DA, Weinstein JA, Ran FA, Konermann S, Agarwala V, et al. DNA targeting specificity of RNA-guided Cas9 nucleases. *Nat Biotechnol*. 2013;31(9):827–32.
34. Doench JG, Fusi N, Sullender M, Hegde M, Vaimberg EW, Donovan KF, et al. Optimized sgRNA design to maximize activity and minimize off-target effects of CRISPR-Cas9. *Nat Biotechnol*. 2016;34(2):184–91.
35. Bae S, Park J, Kim JS. Cas-OFFinder: a fast and versatile algorithm that searches for potential off-target sites of Cas9 RNA-guided endonucleases. *Bioinformatics*. 2014;30(10):1473–5.
36. Sgro A, Blancafort P. Epigenome engineering: new technologies for precision medicine. *Nucleic Acids Res*. 2020;48(22):12453–82.
37. Zhang Z, Xu L, Sun C. Comprehensive characterization of cancer genes in hepatocellular carcinoma genomes. *Oncol Lett*. 2018;15(2):1503–10.
38. Wu L, Guo X, Lyu Y, Clarke SL, Lucas EA, Smith BJ, et al. Targeted metabolomics reveals abnormal hepatic energy metabolism by depletion of beta-carotene oxygenase 2 in mice. *Sci Rep*. 2017;7(1):14624.
39. Liu H, Dong H, Robertson K, Liu C. DNA methylation suppresses expression of the urea cycle enzyme carbamoyl phosphate synthetase 1 (CPS1) in human hepatocellular carcinoma. *Am J Pathol*. 2011;178(2):652–61.
40. Wei L, Liu J, Le XC, Han Y, Tong Y, Lau AS, et al. Pharmacological induction of leukotriene B4–12-hydroxydehydrogenase suppresses the oncogenic transformation of human hepatoma HepG2 cells. *Int J Oncol*. 2011;39(3):735–45.
41. Nwosu ZC, Megger DA, Hammad S, Sitek B, Roessler S, Ebert MP, et al. Identification of the consistently altered metabolic targets in human hepatocellular carcinoma. *Cell Mol Gastroenterol Hepatol*. 2017;4(2):303–23 e1.
42. Fan Y, Wang L, Ding Y, Sheng Q, Zhang C, Li Y, et al. Long non-coding RNA RP4-694A72 promotes hepatocellular carcinoma cell proliferation and metastasis through the regulation of PSAT1. *J Cancer*. 2021;12(18):5633–43.
43. Tada M, Kanai F, Tanaka Y, Tateishi K, Ohta M, Asaoka Y, et al. Down-regulation of hedgehog-interacting protein through genetic and epigenetic alterations in human hepatocellular carcinoma. *Clin Cancer Res*. 2008;14(12):3768–76.
44. Song Y, Tu J, Cheng Y, Zhou F, Liu P, Zhou S, et al. HHIP overexpression suppresses human gastric cancer progression and metastasis by reducing its CpG island methylation. *Front Oncol*. 2020;10:1667.
45. Lin EH, Kao YR, Lin CA, Kuo TY, Yang SP, Hsu CF, et al. Hedgehog pathway maintains cell survival under stress conditions, and drives drug resistance in lung adenocarcinoma. *Oncotarget*. 2016;7(17):24179–93.
46. Agrawal V, Kim DY, Kwon YG. Hhip regulates tumor-stroma-mediated upregulation of tumor angiogenesis. *Exp Mol Med*. 2017;49(1):e289.
47. Bo C, Li X, He L, Zhang S, Li N, An Y. A novel long noncoding RNA HHIP-AS1 suppresses hepatocellular carcinoma progression through stabilizing HHIP mRNA. *Biochem Biophys Res Commun*. 2019;520(2):333–40.
48. Islam SS, Mokhtari RB, Noman AS, Uddin M, Rahman MZ, Azadi MA, et al. Sonic hedgehog (Shh) signaling promotes tumorigenicity and stemness via activation of epithelial-to-mesenchymal transition (EMT) in bladder cancer. *Mol Carcinog*. 2016;55(5):537–51.
49. Della Corte CM, Viscardi G, Papaccio F, Esposito G, Martini G, Ciardiello D, et al. Implication of the Hedgehog pathway in hepatocellular carcinoma. *World J Gastroenterol*. 2017;23(24):4330–40.
50. Liu Q, Lu F, Chen Z. Identification of MT1E as a novel tumor suppressor in hepatocellular carcinoma. *Pathol Res Pract*. 2020;216(11):153213.
51. Bai L, Ren Y, Cui T. Overexpression of CDCA5, KIF4A, TPX2, and FOXM1 coregulated cell cycle and promoted hepatocellular carcinoma development. *J Comput Biol*. 2020;27(6):965–74.
52. Mao J, Yu H, Wang C, Sun L, Jiang W, Zhang P, et al. Metallothionein MT1M is a tumor suppressor of human hepatocellular carcinomas. *Carcinogenesis*. 2012;33(12):2568–77.
53. Ji XF, Fan YC, Gao S, Yang Y, Zhang JJ, Wang K. MT1M and MT1G promoter methylation as biomarkers for hepatocellular carcinoma. *World J Gastroenterol*. 2014;20(16):4723–9.
54. Changjun L, Feizhou H, Dezhen P, Zhao L, Xianhai M. MiR-545-3p/MT1M axis regulates cell proliferation, invasion and migration in hepatocellular carcinoma. *Biomed Pharmacother*. 2018;108:347–54.
55. Xu D, Qu L, Hu J, Li G, Lv P, Ma D, et al. Transmembrane protein 106A is silenced by promoter region hypermethylation and suppresses gastric cancer growth by inducing apoptosis. *J Cell Mol Med*. 2014;18(8):1655–66.
56. Liu J, Zhu H. TMEM106A inhibits cell proliferation, migration, and induces apoptosis of lung cancer cells. *J Cell Biochem*. 2018;120:7825–33.
57. Tsai WC, Hsu PW, Lai TC, Chau GY, Lin CW, Chen CM, et al. MicroRNA-122, a tumor suppressor microRNA that regulates intrahepatic metastasis of hepatocellular carcinoma. *Hepatology*. 2009;49(5):1571–82.
58. Takaki Y, Saito Y, Takasugi A, Toshimitsu K, Yamada S, Muramatsu T, et al. Silencing of microRNA-122 is an early event during hepatocarcinogenesis from non-alcoholic steatohepatitis. *Cancer Sci*. 2014;105(10):1254–60.
59. Wu M, Lan H, Ye Z, Wang Y. Hypermethylation of the PZP gene is associated with hepatocellular carcinoma cell proliferation, invasion and migration. *FEBS Open Bio*. 2021;11(3):826–32.
60. Zhang Z, Li J, He T, Ouyang Y, Huang Y, Liu Q, et al. Two predictive precision medicine tools for hepatocellular carcinoma. *Cancer Cell Int*. 2019;19:290.
61. Zheng Y, Liu Y, Zhao S, Zheng Z, Shen C, An L, et al. Large-scale analysis reveals a novel risk score to predict overall survival in hepatocellular carcinoma. *Cancer Manag Res*. 2018;10:6079–96.
62. Song L, Guo X, Zhao F, Wang W, Zhao Z, Jin L, et al. TTC36 inactivation induce malignant properties via Wnt-beta-catenin pathway in gastric carcinoma. *J Cancer*. 2021;12(9):2598–609.
63. Chai H, Xia L, Zhang L, Yang J, Zhang Z, Qian X, et al. An adaptive transfer-learning-based deep Cox neural network for hepatocellular carcinoma prognosis prediction. *Front Oncol*. 2021;11:692774.
64. Jing W, Peng R, Li X, Lv S, Duan Y, Jiang S. Study on the prognostic values of TTC36 correlated with immune infiltrates and its methylation in hepatocellular carcinoma. *J Immunol Res*. 2022;2022:7267131.
65. Choudhury SR, Cui Y, Lubecka K, Stefanska B, Irudayaraj J. CRISPR-dCas9 mediated TET1 targeting for selective DNA demethylation at BRCA1 promoter. *Oncotarget*. 2016;7(29):46545–56.
66. Wang Q, Dai L, Wang Y, Deng J, Lin Y, Wang Q, et al. Targeted demethylation of the SARI promoter impairs colon tumour growth. *Cancer Lett*. 2019;448:132–43.
67. Xu X, Tao Y, Gao X, Zhang L, Li X, Zou W, et al. A CRISPR-based approach for targeted DNA demethylation. *Cell Discov*. 2016;2:16009.
68. Morita S, Horii T, Kimura M, Hatada I. Synergistic upregulation of target genes by TET1 and VP64 in the dCas9-SunTag platform. *Int J Mol Sci*. 2020;21(5):1574.
69. Liu XS, Wu H, Krzisch M, Wu X, Graef J, Muffat J, et al. Rescue of fragile X syndrome neurons by DNA methylation editing of the FMR1 gene. *Cell*. 2018;172(5):979–92 e6.
70. Huisman C, van der Wijst MG, Schokker M, Blancafort P, Terpstra MM, Kok K, et al. Re-expression of selected epigenetically silenced candidate tumor suppressor genes in cervical cancer by TET2-directed demethylation. *Mol Ther*. 2016;24(3):536–47.
71. Chen H, Kazemier HG, de Groot ML, Ruiters MH, Xu GL, Rots MG. Induced DNA demethylation by targeting ten-eleven translocation 2 to the human ICAM-1 promoter. *Nucleic Acids Res*. 2014;42(3):1563–74.
72. Beltran A, Parikh S, Liu Y, Cuevas BD, Johnson GL, Futscher BW, et al. Re-activation of a dormant tumor suppressor gene maspin by designed transcription factors. *Oncogene*. 2007;26(19):2791–8.
73. Beltran AS, Blancafort P. Reactivation of MASPIN in non-small cell lung carcinoma (NSCLC) cells by artificial transcription factors (ATFs). *Epigenetics*. 2011;6(2):224–35.
74. Perez-Pinera P, Kocak DD, Vockley CM, Adler AF, Kabadi AM, Polstein LR, et al. RNA-guided gene activation by CRISPR-Cas9-based transcription factors. *Nat Methods*. 2013;10(10):973–6.
75. Maeder ML, Linder SJ, Cascio VM, Fu Y, Ho QH, Joung JK. CRISPR RNA-guided activation of endogenous human genes. *Nat Methods*. 2013;10(10):977–9.
76. Wang K, Escobar M, Li J, Mahata B, Goell J, Shah S, et al. Systematic comparison of CRISPR-based transcriptional activators uncovers gene-regulatory features of enhancer-promoter interactions. *Nucleic Acids Res*. 2022;50:7842–55.

77. Broutier L, Mastrogianni G, Versteegen MM, Francies HE, Gavarro LM, Bradshaw CR, et al. Human primary liver cancer-derived organoid cultures for disease modeling and drug screening. *Nat Med*. 2017;23(12):1424–35.
78. Hu B, Li H, Guo W, Sun YF, Zhang X, Tang WG, et al. Establishment of a hepatocellular carcinoma patient-derived xenograft platform and its application in biomarker identification. *Int J Cancer*. 2020;146(6):1606–17.
79. Thakore PI, Kwon JB, Nelson CE, Rouse DC, Gemberling MP, Oliver ML, et al. RNA-guided transcriptional silencing in vivo with *S aureus* CRISPR-Cas9 repressors. *Nat Commun*. 2018;9(1):1674.
80. Beyersdorf JP, Bawage S, Iglesias N, Peck HE, Hobbs RA, Wroe JA, et al. Robust, durable gene activation in vivo via mRNA-encoded activators. *ACS Nano*. 2022;16:5660–71.
81. Lainscek D, Kadunc L, Keber MM, Bratkovic IH, Romih R, Jerala R. Delivery of an artificial transcription regulator dCas9-VPR by extracellular vesicles for therapeutic gene activation. *ACS Synth Biol*. 2018;7(12):2715–25.
82. Chopra M, Sgro A, Norret M, Blancafort P, Iyer KS, Evans CW. SP94-targeted nanoparticles enhance the efficacy of sorafenib and improve liver cancer cell discrimination. *ACS Appl Bio Mater*. 2021;4(1):1023–9.
83. Chopra M, Sgro A, Norret M, Blancafort P, Iyer KS, Evans CW. A peptide-functionalised dendronised polymer for selective transfection in human liver cancer cells. *New J Chem*. 2021;45(41):19315–20.
84. Phipson B, Maksimovic J, Oshlack A. missMethyl: an R package for analyzing data from Illumina's HumanMethylation450 platform. *Bioinformatics*. 2016;32(2):286–8.
85. Maksimovic J, Gordon L, Oshlack A. SWAN: Subset-quantile within array normalization for illumina Infinium HumanMethylation450 BeadChips. *Genome Biol*. 2012;13(6):R44.
86. Robinson MD, McCarthy DJ, Smyth GK. edgeR: a bioconductor package for differential expression analysis of digital gene expression data. *Bioinformatics*. 2010;26(1):139–40.
87. Liu J, Lichtenberg T, Hoadley KA, Poisson LM, Lazar AJ, Cherniack AD, et al. An integrated TCGA pan-cancer clinical data resource to drive high-quality survival outcome analytics. *Cell*. 2018;173(2):400–16 e11.
88. Jones E, Oliphant T, Peterson P. SciPy: open source scientific tools for Python; 2014.
89. McKinney W. Data structures for statistical computing in Python. In: Proceedings of the 9th Python in science conference (SCIPY 2010); 2010.
90. Hunter JD. Matplotlib: a 2D graphics environment. *Comput Sci Eng*. 2007;9(3):90–5.
91. Van Der Walt S, Colbert SC, Varoquaux G. The NumPy array: a structure for efficient numerical computation. *Comput Sci Eng*. 2011;13(2):22–30.
92. Foroutan M, Bhuvana DD, Lyu R, Horan K, Cursons J, Davis MJ. Single sample scoring of molecular phenotypes. *BMC Bioinform*. 2018;19(1):404.
93. Pedregosa F, Varoquaux G, Gramfort A, Michel V, Thirion B, Grisel O, et al. Scikit-learn: machine learning in Python. *J Mach Learn Res*. 2011;12(85):2825–30.
94. Robinson MD, Oshlack A. A scaling normalization method for differential expression analysis of RNA-seq data. *Genome Biol*. 2010;11(3):R25.
95. Schmittgen TD, Livak KJ. Analyzing real-time PCR data by the comparative C(T) method. *Nat Protoc*. 2008;3(6):1101–8.
96. Ritchie ME, Phipson B, Wu D, Hu Y, Law CW, Shi W, et al. Limma powers differential expression analyses for RNA-sequencing and microarray studies. *Nucleic Acids Res*. 2015;43(7):e47.
97. McCarthy DJ, Smyth GK. Testing significance relative to a fold-change threshold is a TREAT. *Bioinformatics*. 2009;25(6):765–71.

Publisher's Note

Springer Nature remains neutral with regard to jurisdictional claims in published maps and institutional affiliations.

Ready to submit your research? Choose BMC and benefit from:

- fast, convenient online submission
- thorough peer review by experienced researchers in your field
- rapid publication on acceptance
- support for research data, including large and complex data types
- gold Open Access which fosters wider collaboration and increased citations
- maximum visibility for your research: over 100M website views per year

At BMC, research is always in progress.

Learn more biomedcentral.com/submissions

